SIMULATION OF NATURALLY FRACTURED RESERVOIRS USING EMPIRICAL TRANSFER FUNCTIONS

A Thesis

by

PRASANNA K. TELLAPANENI

Submitted to the Office of Graduate Studies of
Texas A&M University
in partial fulfillment of the requirements for the degree of

MASTER OF SCIENCE

December 2003

Major Subject: Petroleum Engineering

SIMULATION OF NATURALLY FRACTURED RESERVOIRS USING EMPIRICAL TRANSFER FUNCTIONS

A Thesis

by

PRASANNA K. TELLAPANENI

Submitted to the Office of Graduate Studies of
Texas A&M University
in partial fulfillment of the requirements for the degree of

MASTER OF SCIENCE

Approved as to style and content by:

David S. Schechter (Chair of Committee)	Wayne Ahr (Member)
Duane A. McVay (Member)	Hans Juvkam-Wold (Head of Department)

December 2003

Major Subject: Petroleum Engineering

ABSTRACT

Simulation of Naturally Fractured Reservoirs Using Empirical Transfer Functions.

(December 2003)

Prasanna K. Tellapaneni, B. Tech., Indian School of Mines

Chair of Advisory Committee: Dr. David. S. Schechter

This research utilizes the imbibition experiments and X-ray tomography results for modeling fluid flow in naturally fractured reservoirs. Conventional dual porosity simulation requires large number of runs to quantify transfer function parameters for history matching purposes. In this study empirical transfer functions (ETF) are derived from imbibition experiments and this allows reduction in the uncertainness in modeling of transfer of fluids from the matrix to the fracture.

The application of the ETF approach is applied in two phases. In the first phase, imbibition experiments are numerically solved using the diffusivity equation with different boundary conditions. Usually only the oil recovery in imbibition experiments is matched. But with the advent of X-ray CT, the spatial variation of the saturation can also be computed. The matching of this variation can lead to accurate reservoir characterization. In the second phase, the imbibition derived empirical transfer functions are used in developing a dual porosity reservoir simulator. The results from this study are compared with published results. The study reveals the impact of uncertainty in the transfer function parameters on the flow performance and reduces the computations to obtain transfer function required for dual porosity simulation.

DEDICATION

To my beloved parents, my brother, Kiran, and to all my friends, for their love, care, and inspiration.

ACKNOWLEDGMENTS

I would like to express my deepest gratitude to all who have assisted me during my studies and research. I would especially like to thank my advisor, Dr. David S. Schechter, for his continuous trust and encouragement.

I would also like to thank Dr. Duane McVay and Dr. Wayne Ahr for acting as committee members and helping me in my research.

Finally, I want to thank my friends in the naturally fractured reservoir group: Dr. Erwin Putra for his friendliness and technical help, Sandeep P. Kaul, Vivek Muralidharan and Deepak Chakravarthy for making my years as a graduate student pleasurable. I would also like to acknowledge the facilities provided by the Harold Vance Department of Petroleum Engineering, Texas A&M University.

Thank you very much.

TABLE OF CONTENTS

Page

Page

LIST OF FIGURES

Page

LIST OF TABLES

Page

CHAPTER I
INTRODUCTION

1.1 Naturally Fractured Reservoirs (NFRs)

Fractures are defined as "a macroscopic planar discontinuity in rock which is interpreted to be due to deformation or diagenesis[1]". These fractures may be due to compactive or dilatent processes and may have a positive or negative impact on fluid flow. Naturally fractured reservoir can be defined as any reservoir in which naturally occurring fractures have, or are predicted to have, a significant effect of flow rates, anisotropy, recovery or storage. The porous system of any reservoir can usually be divided into two parts:

- Primary Porosity: - This porosity is usually inter-granular and is controlled by lithification and deposition.
- Secondary Porosity: - Post lithification processes cause this porosity.

The post-lithification processes that cause secondary porosity are general in the form of solution, recrystallization, dolomotization, fractures or jointing. Naturally fractured reservoirs form a challenge to the reservoir-modeling world due to its complexities. Substantial research has been accomplished in the area of geo-mechanics, geology and reservoir engineering of fractured reservoirs.[2, 3, 4, 5, 6] Recently[7] new areas of research are being explored, including the origin and development of fracture systems, fracture detection methods, efficient numerical modeling of fluid flow and methodologies to test these models.

1.2 Dual Porosity Method of Modeling Fluid Flow in NFRs

In a NFR, the primary porosity contributes significantly to fluid storage but negligibly to fluid flow whereas the secondary porosity has a significant impact on fluid flow and no

---

This thesis follows style of *Journal of Petroleum Technology*.

or very less role in fluid storage. Hence dual porosity formulation was developed. This formulation consists of a dichotomy of the internal pores as follows:

- Primary Porosity (Matrix): - Matrix is the portion of the porous system that is the inter-granular and controlled by deposition methods. This media contributes significantly to fluid storage but because of low permeability, its contribution to fluid flow is low.
- Secondary Porosity (Fracture): - Fractures are the portion of the porous system that is caused by fractures, solution or other post-depositional phenomenon. These are highly permeable and hence contribute significantly to the fluid flow but as they are not very porous, their contribution to fluid storage is negligible.

Most of the petroleum reservoirs show dichotomy of porous space but with varying degree of matrix and fracture presence. A low fractured reservoir is one in which the fracture media is not significant. But most NFRs are highly fractured and consist of a significant amount of secondary porosity. Hence this dichotomy for NFRs is justified. Dual porosity formulation superimposes the secondary or fracture media on the primary or matrix media and this superimposition is idealized as primary porosity coupled with the secondary porosity as shown in **Fig 1.1.** The following are the main assumptions made in dual porosity formulation:

- The matrix blocks are isotropic and homogeneous.
- The secondary porosity can be idealized as orthogonal, uniform and continuous sets of fractures that are parallel to the principle axes of permeability.
- Flow occurs only through the secondary porosity although flow through the primary porosity to the secondary porosity is possible.

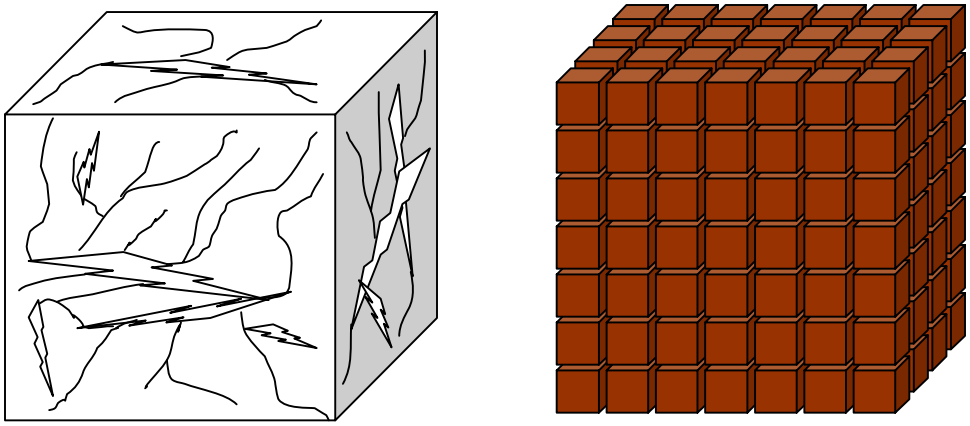

(a) Actual Reservoir (b) Ideal Reservoir.

Fig. 1.1- Idealization of dual porosity reservoir[21].

Most of the research in terms of naturally fractured reservoirs has been done to model accurately the inter-porosity flow between the matrix and the fracture continua. NFRs are characterized by very high initial production and after a very brief period of time they reach a plateau in the production. This plateau is controlled by the inter-porosity flow between the matrix and the fracture. Hence efficient modeling of this phenomenon is necessary for efficient reservoir modeling. Also in the modeling of secondary and tertiary production schemes, the inter-porosity flow plays an important role. But the inter-porosity flow is highly complex to model and therefore there are large number of phenomenons proposed by various workers to idealize this flow. Some of the main phenomenons:

- Gravity and Capillary effects[8, 9]
- Reinflitration[10, 11]
- Capillary Continuity[12, 13]
- Counter-Current and Co-Current Imbibition[14, 15]

Some field and laboratory observations have been studied through numerical simulation, which typically assumes that there are two continua, matrix and fractures, within each simulation grid-block. Flow equations are written for each system with a

matrix/fracture transfer function to relate the loss or gain of matrix fluids to or from the fracture (inter-porosity flow). This fluid transfer rate is commonly calculated as a function of the pressure difference between the matrix and fracture systems, matrix flow capacity and matrix geometry considered through a constant shape factor. However, in spite of the great level of current model sophistication, the highly anisotropy and heterogeneous nature of a fractured formation makes fractured reservoir modeling a challenging task, frequently with uncertain results in forecasting.

This study uses the counter-current imbibition phenomenon to model inter-porosity flow. This model allows integration of the laboratory imbibition experiments and dual porosity simulation to simulate fluid flow. This approach is shown to be an improved way to model naturally fractured formations because it translates laboratory experiments into inter-porosity flow. The definition of naturally fractured reservoirs can be extended, without loss of generality, to any reservoir in which secondary porosity is significant[16,17].

In this report the study has been divided into chapters. In chapter II, a detailed literature review of the present models to simulate fluid flow in NFRs is presented. Chapter III consists of derivation of the lab experiment modeling and integration of these experiments with dual porosity formulations. Relevant equations are used to describe both the numerical modeling of the imbibition experiments and also the proposed dual porosity formulation. In chapter IV, imbibition experiments are modeled and the extension to dual porosity formulations is tested using a commercially available simulator. Chapter V details the conclusions derived from this study.

CHAPTER II

LITERATURE REVIEW

With increasing number of deep-water exploration, more number of fractured, vuggular and heterogeneous reservoirs are being explored and developed. This has increased the attention of the petroleum industry towards unconventional and fractured reservoir modeling. With the advent of faster computers with large amount of memory space, the industry is now able to model complex reservoirs faster and with much accuracy. In this section, commonly used approaches for naturally fractured reservoir modeling and inter-porosity flow estimation are reviewed and analyzed.

2.1 Fluid Flow Modeling in NFRs

Modeling of fluid flow in naturally fractured reservoirs can be broadly classified into the following models[7]:

1. Discrete Fracture Network Models.
2. Equivalent Continuum Models.
3. Hybrid Models.

Discrete networks consist of modeling of a population of fractures. Equivalent continuum methods, model reservoirs by assigning equivalent rock and fluid parameters to large rock masses. Hybrid models are a combination of both discrete fracture networks and equivalent continuum methods. The selection of any particular model depends, not only on the reservoir and the type of fluid flow behavior to be numerically simulated, but also on the amount of computer memory and speed available for the project. Due to the ease of computation, the equivalent continuum modeling approach is the most favored to model fluid flow in NFRs. But whenever models are to be solved very accurately with very reliable data, the other two models may be applied. It has been shown that the equivalent continuum methods are sufficient to model reservoir rocks that have undergone multiple and extensive deformations (high fracture density) and/or any formations where matrix permeabilities are large enough that fluid flow is not influenced

by any individual fracture or series of fractures that form a conducting channel[18]. Because of the relevance to this study, the most important equivalent continuum models – single-porosity and dual-porosity models – are briefly reviewed.

2.1.1 Single Porosity Modeling

Single porosity modeling is the most common method of modeling non-fractured reservoirs. This model does not differentiate between the matrix and fracture continua and equivalent rock and fluid properties are assigned to both the continuum. Since this methodology doesn't differentiate between the continua, this is the most accurate modeling method. But its accuracy is dependent on the number of grid-blocks used therefore can lead to large computational times.

Agarwal *et al.*[19] have used the single continuum method to model a carbonate reservoir with large number of fractures in the North Sea. To circumvent the problem of computation, Agrawal used psuedo-relative permeability functions. To generate these curves, dual porosity simulation was done on a stack of matrix blocks and matched with fine grid simulation. This method receives special consideration because of the ease of computation and accuracy generated by this methodology. This methodology, however, cannot be used for reservoir management as new sets of dynamic pseudo-functions had to be calculated for every change in operating conditions.

2.1.2 Dual Porosity Modeling

Dual porosity simulation is the most commonly used method for fluid flow modeling in reservoirs with significant secondary porosity. In general, to model fluid flow in NFRs, it is necessary to spatially define the secondary porosity. Since secondary porosity is inherently complex and cannot be easily quantified, an idealization is made. This idealization was initially proposed by Barenblatt *et al.*[20] for single-phase fluid flow and consisted of dividing the porous media in two superimposed continua, a continuous continuum of fractures (secondary porosity) and a discontinuous matrix (primary porosity) continuum. The fracture system is further assumed to be the primary flow paths but have negligible storage capacity. Also the matrix is assumed to be the storage medium of the system with negligible flow capacity. Warren and Root[21] who presented an analytical solution for the single-phase radial flow in a reservoir with significant

secondary introduced this idealization to the petroleum engineering. The idealization made the following assumptions:

- The primary porosity is isotropic and is contained in a symmetric array of identical parallelepipeds.
- All the secondary porosity is contained in a set of orthogonal fractures, which are oriented in a direction parallel to the axis of permeability.
- Flow can occurs in the secondary porosity and from the primary porosity to the secondary porosity but not in the primary porosity.

The idealization can be visualized as in **Fig. 1.1**. Both the primary and fracture media are consistent in neither orientation nor continuity in **Fig. 1.1 (a)**, which is the actual reservoir. This actual reservoir is idealized as shown in **Fig. 11 (b)**. The idealized reservoir can be viewed as a series of primary porosity contained in the parallelepipeds, which are disconnected from each other, by a series of continuous secondary porosities. Other idealizations include parallel horizontal fracture[22] and matchstick column[4] models. Multi-porosity models are a special case of dual porosity models, which assume that the fracture set interacts with two groups of matrix blocks with distinct permeabilities and porosities[23].

2.2 Transfer Function

The primary and secondary porosities are coupled by a factor called the transfer function or the inter-porosity flow. Physically, this can be defined as the rate of fluid flow between the primary and the secondary porosities. Since the secondary porosity is the only fluid path and it lacks in fluid storage, the dual porosity simulation method can be imagined as a system of secondary porosity with the primary porosity as the only source of fluids. The transfer function can be regarded as the "heart" of dual porosity since it is the parameter that is changed to effect the transition from the actual reservoir as shown in **Fig. 1.1 (a)** to the ideal reservoir as shown in **Fig. 1.1 (b)**. Transfer functions can be broadly classified to be of four types:

1. Empirical Transfer Functions.
2. Scaling Transfer Functions.
3. Diffusivity Transfer Functions.
4. Transfer Functions That Use Darcy Law.

2.2.1 Empirical Transfer Functions

Empirical models assume the transfer or inter-porosity flow can be attributed to imbibition phenomenon. They assume an exponential decline function to describe the time rate of exchange of oil and water for a single matrix block when surrounded by fractures with high water saturation. Empirical transfer functions usually consist of two parts:

1. A curve fitting expression to express recovery as a function of time.
2. A scaling equation to express the time in terms of rock and fluid properties.

The first empirical oil recovery function was given by Aronofsky[24]. He showed that the rate of transfer of fluids from the matrix can be approximated by an exponential decline function as shown

$$R = R_{\infty}(1 - e^{-\lambda t}) \tag{2.1}$$

deSwaan[25] used the above relation to derive an analytical expression for the water oil ratio and the cumulative oil production from a linear reservoir with water flooding. His theory also accounts for the fact that in a reservoir exploited by water flooding, the matrix blocks downstream from the waterfront are subject to varying degree of saturation of fractures due to the water imbibition of the matrix blocks upstream. His theory modifies the well-known Buckley-Leverett formulation by addition of a term for the interporosity flow or transfer function.

$$-\frac{\partial q}{\partial x} = h\phi\frac{\partial S_w}{\partial t} + \frac{N_{ma}}{\tau_1}\int_o^t e^{-(t-\theta)/\tau 1}\frac{\partial S_w}{\partial \theta}d\theta \tag{2.2}$$

Also assuming that the fractional flow coefficient is the same as the mobile water saturation, he derived an analytical solution for the above equation. The analytical solution contains an integro-differential term as shown below.

$$S_w = \begin{cases} 0, t < t_{Lf} \\ 1 - e^{-t/\tau} \int e^{-y} I_o(2\sqrt{ty/\tau}) dy, t > t_{LF} \end{cases} \quad (2.3)$$

Kazemi *et al.*[26] solved the analytical expression derived by deSwaan by using explicit finite difference and trapezoidal rule. Reis and Cil[27] proposed a new relation for oil recovery function

$$R = R_\infty (1 - e^{-0.69(\lambda t)^n}) \quad (2.4)$$

Civan[28] extended the arfonsky relation by addition of an exponential term as shown in equation 2.5.

$$R = R_\infty (1 - e^{-\lambda t_1} - e^{-\lambda_2 t}) \quad (2.5)$$

The second exponential term was justified by the fact that the collection of oil droplets in the fracture consist of two different irreversible processes, namely:

1. Expulsion of oil droplets from the matrix into the fracture.
2. Entraining of the oil droplets in the fracture by the fluid present in the fracture.

The equation 2.5 was used in the Buckley-Leverett equation similar to deSwaan and a numerical solution was developed. This numerical solution used the quadrature solution. He showed that the quadrature solutions are easily computed than the finite difference solutions for the case of end point mobilites. Civan and Gupta[29] proposed an additional term to the equation 2.5 as shown below

$$R = R_\infty (1 - e^{-\lambda t_1} - e^{-\lambda_2 t} - e^{-\lambda_3 t}) \quad (2.6)$$

The third term was added to include the “dead-end” pores of the matrix but the results obtained did not justify the need for the inclusion of this third term[30]. The above said empirical methods suffer from the following limitations:

1. This method is limited to water flooded reservoirs.
2. The capillary pressure role in oil recovery is neglected.
3. Gravity is neglected.
4. This method is limited to two phases only.

2.2.2 Scaling Transfer Functions

Scaling transfer functions are used to predict recovery in field size cases with the results from lab experiments. Rapoport[31] proposed the "scaling laws" applicable in case of water-oil flow. Using these laws Mattax and Kyte[32] presented the dimensionless time to scale up laboratory data to field size cases. The dimensionless time is given as

$$t_D = t\sqrt{k/\phi}\left(\frac{\sigma}{\mu_w L^2{}_c}\right) \tag{2.7}$$

Du Prey[33] performed imbibition experiments on cores within centrifuges to account for gravity effect on imbibition. He showed that the dimensionless time defined by the previous equation couldn't be used to model the experiments. He also showed that the dimensionless equation 2.7 couldn't be used for matrix blocks of different sizes. He defined three more dimensionless parameters:

- Dimensionless Shape factor
- Dimensionless mobility
- Capillary to gravity ratio

The dimensionless time was defined for two cases: namely, low capillary to gravity ratio and for high capillary to gravity ratio. His definitions are as follows

$$t_c = \frac{H^2 \phi \Delta S \mu_o}{P_{ct} k_{o\max}}$$
$$t_g = \frac{H\ \phi \Delta S \mu_o}{\Delta \rho g k_{o\max}} \tag{2.8}$$

Where

t_c Dimensionless time factor for high capillary gravity ratio

t_g Dimensionless time factor for low capillary gravity ratio

Ma *et al.*[34] studied the relationship between water wetness and the oil recovery from imbibition. The characteristic length to scale up time was also defined for various cases. The authors also defined "effective viscosity" to remove the condition of comparable viscosities between the lab and field cases.

$$t_D = t\sqrt{\frac{k}{\phi}}\frac{\sigma}{\mu_g}\frac{1}{L_c^2} \tag{2.9}$$

Where

$$\mu_g = \sqrt{\mu_w \mu_{nw}} \tag{2.10}$$

Although the scaling transfer functions are the best transfer function representations, the following are the requirements for the correct formulation of scaling transfer functions:

1. The shapes of the matrix blocks of the field and lab cases must be of the same shape.
2. The fluid mobilites must be comparable.
3. The initial and boundary conditions for both the lab and matrix cases must be the same.
4. The capillary pressures must be directly proportional

Because of these inherent assumptions the scaling transfer functions are not widely used.

2.2.3 Transfer Function Using Darcy's Law

Transfer functions that use "Darcy's Law", assume that the transfer of fluids from the matrix to the fracture can be adequately be described by Darcy's law with an appropriate geometric factor that accounts for the characteristic length and the flow area between the matrix and the fracture.

The first model was proposed by Barenblatt *et al.* which is analgous to a model used for heat transfer in a heterogeneous medium. They assumed that the outflow of fluids from matrix blocks into the fractures is steady-state and that the fluid transfer rate is a

function of the viscosity of the fluid, the pressure drop between the matrix and fracture systems, and matrix-rock properties related to geometry and porous interconnectivity in the matrix block. According to Barenblatt *et al.*, the fluid transfer rate per unit volume of rock is calculated from the following expression:

$$q = \frac{\sigma K_m}{\mu}(p_m - p_f) \tag{2.11}$$

Where σ is a shape factor related to the specific surface of the fractures, p_m and p_f are the average pressures in the matrix and fracture domains, respectively, and q is the fluid transfer rate between the matrix and fracture. Although this transfer function is the most popular, there is hardly any agreement between various researchers regarding the shape factor. Bourbiaux *et al.*[35] presented a comparison of shape factors found in the literature. **Table 2.1** is a modified version of the Bourbiaux table as reported by Penula-Pineda[36]. Although the transfer functions of this family are the most popular they suffer from the following limitations:

1. These assume a linear gradient of pressures between the matrix and the fractures centers.
2. They also assume that the whole storage is present in the matrix blocks only.
3. These transfer functions lack a lab background that the other methods enjoy.
4. They also assume that all the matrix blocks exist at the same saturation.
5. Recovery from “n” number of matrix blocks is equal to “n” times the recovery from a single matrix blocks.
6. Linear relative permeability is assumed in the fracture media.

Table 2.1- Shape Factors as Reported by Penula-Pineda.

Mathematical Approximations	Slab Geometry	**Square Geometry**	**Cube Geometry**
Warren And Root	12	32	60
Kazemi *et al.*	4	8	12
Thomas *et al.*[37]	-	-	25
Coats[38]	8	16	24
Kazemi and Gilman[39]	-	-	29.6
Limm and Aziz[40]	9.9	19.7	29.6
Quintard and Whitaker[41]	12	28.4	49.6
Noetinger *et al.*[42]	11.5	27.1	-
Bourbiaux *et al.*	-	20	-

2.2.4 Diffusivity Transfer Functions

These transfer functions assume that the inter-porosity flow can be approximated by "diffusion" phenomenon. These functions are based on incompressible flow and assume that diffusivity equation[43] is sufficient to model the inter-porosity flow between the matrix and the fracture media. Hernandez and Rosales[44] proposed the first diffusivity transfer function. They developed an analytical equation for the oil production from water flooded reservoirs and verified the same from imbibition experiments on Berea cores.

$$N_{pn} = 1 - \frac{8}{\pi^2} \sum_{n=0}^{\alpha} \frac{1}{(2n+1)^2} \exp[-(2n+1)^2 t_D] \qquad (2.12)$$

Hayashi and Rosales[45] developed a technique for making visual observations of water imbibition processes in porous media saturated with oil. They found that the spontaneous penetration of the water by imbibition was similar to diffusion phenomenon. Also based

on experimental results, a theoretical model is proposed for explaining imbibition processes.

$$N_{pn} = 1 - [\frac{8}{\pi^2} \sum_{n=0}^{\alpha} \frac{1}{(2n+1)^2} \exp[-\frac{D(2n+1)^2 \pi^2 t}{L^2}\ ]^2 \qquad (2.13)$$

D is a coefficient to be estimated by trial and error.

The transfer functions of this family suffer from the following limitations:

1. They assume diffusion phenomenon is sufficient for inter-porosity flow.
2. This method can be used only for two-phase (water-oil) cases.
3. Compressibility of fluids is ignored.

2.2 Comparison of Transfer Functions

Reis and Cil[27] have made comparisons between the various transfer functions on several imbibition experiments with different boundary conditions and found the following:

1. The match between the diffusivity models and the experimental data were found to be good except at early times.
2. The scaling function was found to match the experiments within experimental errors.
3. The empirical function was found to have a good agreement with the experimental values.

For single-phase inter-porosity flow, Najurieta[46] showed that deSwaan's analytical model results were equivalent to numerical solutions provided by Kazemi, which accounted for pressure transient effects by assuming non-steady state flow at the matrix/fracture interface.

The procedure developed in this study is intended for implementation in existing simulators without significantly increasing computational work while representing pressure transient and saturation gradient effects on the inter-porosity flow as accurately

as possible. In the following chapter, the conceptual model that is the basis for this procedure is presented.

2.3 Flow Visualization Using X-ray Tomography

Computerized tomography is a non-destructive technique that utilizes X-rays and mathematical reconstruction algorithms to generate a cross-sectional slice of an object[47]. Hounsfield[48] patented the first X-ray CT technique and was initially used for medical purposes. The applications of X-ray CT in the petroleum industry have ranged from detection of rock heterogenties[49, 50,51] to determination of bulk densities[52]. But the main use of CT has been found in flow visualization.

A detailed explanation of the principles and application of X-ray CT can be found in the literature[49].

CHAPTER III
FORMULATION OF MODELS

The objective of this chapter is to derive the formulations for:

1. Diffusivity Equations that are used to model imbibition experiments.
2. Derivation of empirical transfer function from imbibition experiments.

3.1 Derivation of the Diffusivity Equation

3.1.1 Conservation of Mass

From Darcy's Law for multiphase flow in a porous media, we have that

$$\vec{u}_w = -\frac{k\,k_{rw}}{\mu_w}\nabla\Phi_w = -\frac{k\,k_{rw}}{\mu_w}\nabla(p_w + \rho_w g h) \tag{3.1}$$

$$\vec{u}_o = -\frac{k\,k_{ro}}{\mu_o}\nabla\Phi_o = -\frac{k\,k_{ro}}{\mu_o}\nabla(p_o + \rho_o g h) \tag{3.2}$$

From the definition of capillary pressure, the water phase pressure can be expressed in terms of oil phase pressure as

$$P_c = p_o - p_w = P_c(S_w); \qquad p_w = p_o - P_c \tag{3.3}$$

Thus 3.1 can be re-written as

$$\vec{u}_w = -\frac{kk_{rw}}{\mu_w}\nabla(p_o - P_c + \rho_w g h) \tag{3.4}$$

Consider a control volume of dimensions Δx, Δy as shown in **Fig. 3.1**.

From conservation of mass principle, we have that

[Rate of change of mass in Control Volume = Rate of Net Influx]

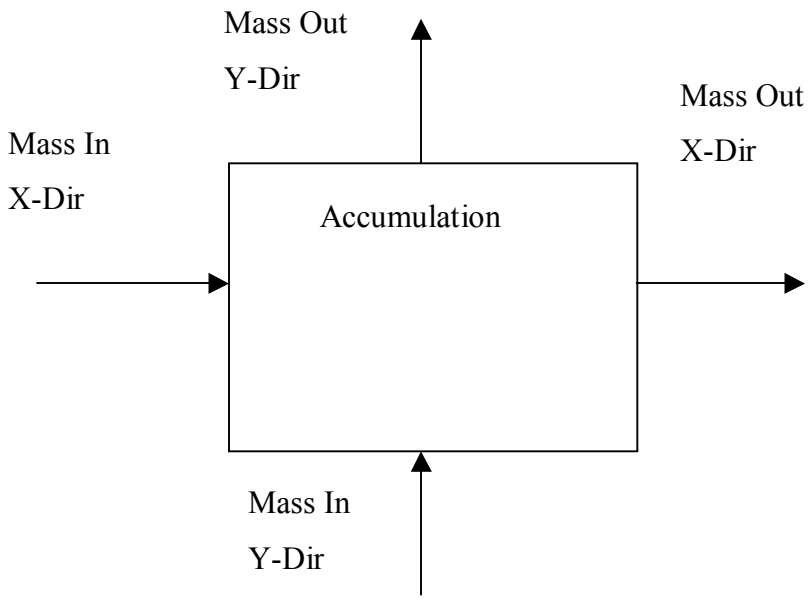

Fig. 3.1- Conservation of mass in a control volume.

Consider the control volume in Fig 3.1, for the phase water we have

Rate of change of mass of water in X direction

$$\rho_w \vec{u}_{wx} \Delta y - (\rho_w \vec{u}_{wx} + \frac{\partial}{\partial x}(\rho_w \vec{u}_{wx})\Delta x)\Delta y$$

Similarly for the Y direction

$$\rho_w \vec{u}_{wy} \Delta x - (\rho_w \vec{u}_{wy} + \frac{\partial}{\partial x}(\rho_w \vec{u}_{wy})\Delta y)\Delta x$$

Rate of accumulation of water

$$\frac{\partial}{\partial t}(\phi S_w \rho_w \Delta x \Delta y)$$

Thus the conservation of mass can be written in the following form

$$\frac{\partial}{\partial t}(\phi S_w \rho_w \Delta x \Delta y) = (\rho_w \vec{u}_{wy} \Delta x - (\rho_w \vec{u}_{wy} + \frac{\partial}{\partial x}(\rho_w \vec{u}_{wy})\Delta y)\Delta x) + (\rho_w \vec{u}_{wx} \Delta y - (\rho_w \vec{u}_{wx} + \frac{\partial}{\partial x}(\rho_w \vec{u}_{wx})\Delta x)\Delta y) \quad (3.5)$$

$$\frac{\partial}{\partial t}(\phi S_w \rho_w \Delta x \Delta y) = \frac{\partial}{\partial x}(\rho_w \vec{u}_{wy})\Delta y \Delta x + \frac{\partial}{\partial x}(\rho_w \vec{u}_{wx})\Delta x \Delta y \quad (3.6)$$

$$\frac{\partial}{\partial t}(\phi S_w \rho_w)\Delta x\Delta y = \frac{\partial}{\partial x}(\rho_w \vec{u}_{wy})\Delta y\Delta x + \frac{\partial}{\partial x}(\rho_w \vec{u}_{wx})\Delta x\Delta y \tag{3.7}$$

$$\phi\frac{\partial}{\partial t}(S_w \rho_w) = \frac{\partial}{\partial x}(\rho_w \vec{u}_{wy}) + \frac{\partial}{\partial x}(\rho_w \vec{u}_{wx}) \tag{3.8}$$

$$\phi\frac{\partial}{\partial t}(S_w) = \nabla.(\vec{u}_w) \tag{3.9}$$

Similarly for oil phase we have

$$\phi\frac{\partial}{\partial t}(S_o) = \nabla.(\vec{u}_o) \tag{3.10}$$

Adding 1.9 and 1.10 we have

$$\phi\frac{\partial}{\partial t}(S_o + S_w) = \nabla.(\vec{u}_o + \vec{u}_w) \tag{3.11}$$

But by definition we have that the sum of saturations is one. Therefore 3.11 can be written as

$$\nabla.(\vec{u}_o + \vec{u}_w) = 0 \tag{3.12}$$

3.1.2 Diffusivity Equation

Substituting equation 3.1 and 3.2 in 3.12 we have

$$\nabla.(-\frac{kk_{rw}}{\mu_w}\nabla(p_o - P_c + \rho_w gh) - \frac{kk_{ro}}{\mu_o}\nabla(p_o + \rho_o gh)) = 0 \tag{3.13}$$

Defining mobilites as

$$\lambda_o = \frac{kk_{ro}}{\mu_o}; \lambda_w = \frac{kk_{rw}}{\mu_w}; \lambda_T = \lambda_w + \lambda_o \tag{3.14}$$

Substituting in 3.13 and rearranging terms we have

$$\nabla.(\lambda_T \nabla p_o - \lambda_w \nabla P_c + (\lambda_o \rho_o + \lambda_w \rho_w)g\nabla h) = 0 \tag{3.15}$$

Now neglecting gravity terms we have

$$\nabla.(\lambda_T \nabla p_o - \lambda_w \nabla P_c) = 0 \tag{3.16}$$

$$\nabla.(\nabla p_o - \frac{\lambda_w}{\lambda_T}\nabla P_c) = 0 \tag{3.17}$$

$$\nabla.(\nabla p_o) = \nabla.(\frac{\lambda_w}{\lambda_T}\nabla P_c) \tag{3.18}$$

From equation 3.10 we have that

$$\phi\frac{\partial}{\partial t}(S_o) = \nabla.(\vec{u}_o) \tag{3.19}$$

$$\phi\frac{\partial}{\partial t}(S_o) = \nabla.(\lambda_o\nabla p_o) \tag{3.20}$$

$$-\phi\frac{\partial}{\partial t}(S_w) = \nabla.(\lambda_o\nabla p_o) \tag{3.21}$$

$$-\phi\frac{\partial}{\partial t}(S_w) = \nabla.(\lambda_o\nabla(\frac{\lambda_w}{\lambda_T}P_C)) \tag{3.22}$$

$$\nabla.(\frac{\lambda_o\lambda_w}{\lambda_T}\nabla P_C) + \phi\frac{\partial}{\partial t}(S_w) = 0 \tag{3.23}$$

$$\nabla.(\frac{\lambda_o\lambda_w}{\lambda_T}\frac{dP_C}{dS_w}\nabla S_w) + \phi\frac{\partial}{\partial t}(S_w) = 0 \tag{3.24}$$

$$\nabla.(D\nabla S_w) + \frac{\partial}{\partial t}(S_w) = 0 \tag{3.25}$$

Where

$$D = (\frac{\lambda_o + \lambda_w}{\phi\lambda_T})\frac{dP_c}{dS_w}$$

3.1.3 Discretization of the Diffusivity Equation

3.1.3.1 Initial and Boundary Conditions

Equation 3.25 is the final form of the diffusivity equation. In order to simulate the core imbibition experiments, boundary and initial conditions are required. The following are the initial and boundary conditions used.

Initial Condition

$$S_w(x,y,t) = 1 - S_{oi}, t = 0 \tag{3.26}$$

Boundary Condition

Depending on the boundaries modeled the boundary condition as shown below can be utilized. For example if the core is completely surrounded by the wetting phase then the boundary condition would be

$$\begin{aligned} &S_w(x,y,t) = 1, x = 0 \\ &S_w(x,y,t) = 1, y = 0 \\ &S_w(x,y,t) = 1, y = L_y \\ &S_w(x,y,t) = 1, x = L_x \end{aligned} \tag{3.27}$$

And if the core is surrounded by the wetting phase only at the bottom as in Garg *et al.* case then the boundary conditions are as follows

$$S_w(x,y,t) = 1, y = 0 \tag{3.28}$$

3.1.3.2 Finite Difference Form of Diffusivity Equation

Consider a spatial control volume that has been divided into a mesh of grid blocks of equal dimensions Δx. and Δy (two dimensions) as shown in **Fig. 3.2**. So the objective of this exercise is to discretize equation 1.25 on this control volume.

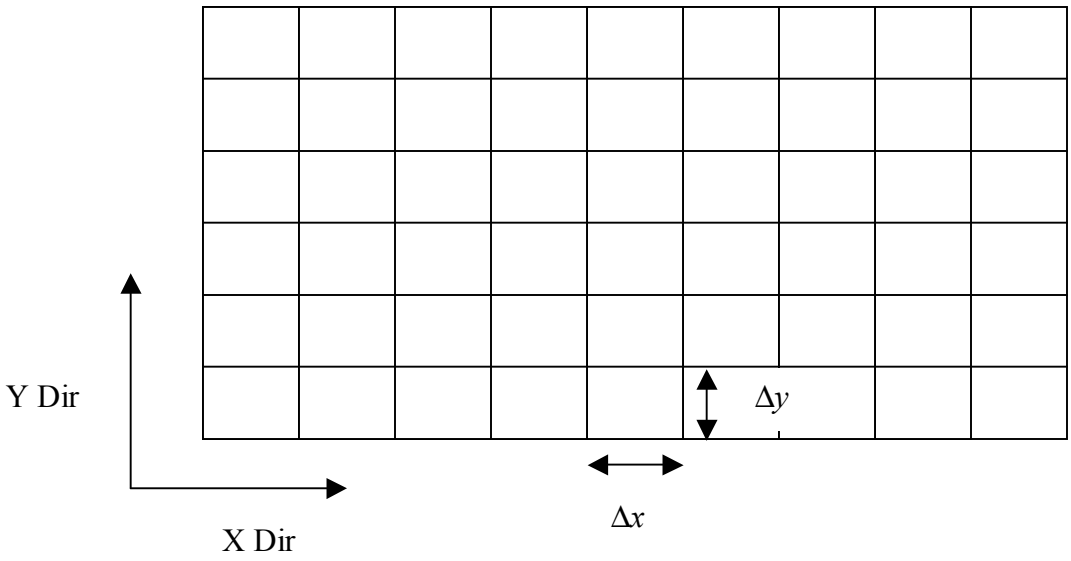

Fig. 3.2- Example gridded control volume.

By definition Taylor's Series can be written as

$$f(x+\Delta x) = f(x) + \Delta x \frac{\partial f}{\partial x} + O(\Delta x^2)$$

$$f(x+\Delta x) = f(x) + \Delta x \frac{\partial f}{\partial x} + \Delta x^2 \frac{\partial^2 f}{\partial x^3} + O_1(\Delta x^3) \tag{3.30}$$

Where

O(x) is the truncation error of order 2.

$O_1(x)$ is the truncation error of order 3.

Thus rewriting 3.29 to obtain the partial derivative we have that

$$\frac{\partial f}{\partial x} = \frac{f(x+\Delta x) - f(x)}{\Delta x} \tag{3.31}$$

Also using Taylor's Series, we can also write

$$f(x+\Delta x) = f(x) + \Delta x \frac{\partial f}{\partial x} + \frac{\Delta x^2}{2!} \frac{\partial^2 f}{\partial x^3} + O_1(\Delta x^3) \tag{3.32}$$

$$f(x-\Delta x)=f(x)-\Delta x\frac{\partial f}{\partial x}+\frac{\Delta x^2}{2!}\frac{\partial^2 f}{\partial x^2}+O_1(\Delta x^3) \tag{3.33}$$

adding 3.33 and 3.34 we have that

$$f(x-\Delta x)+f(x+\Delta x)=2f(x)+2\frac{\Delta x^2}{2!}\frac{\partial^2 f}{\partial x^2}+O_1(\Delta x^3) \tag{3.34}$$

$$\frac{\partial^2 f}{\partial x^2}=\frac{f(x-\Delta x)+f(x-\Delta x)-2f(x)}{\Delta x^2} \tag{3.35}$$

Thus from equation 3.31 we have that

$$\frac{\partial S_w}{\partial t}=\frac{S_w{}^{n+1}-S_w{}^{n}}{\Delta t} \tag{3.36}$$

Where

n	Time step
n + 1	Incremented time step

Also,

$$\begin{aligned}\frac{\partial S_w}{\partial x}&=\frac{S_{w,i+1}-S_{wi}}{\Delta x}=\frac{S_{wi}-S_{wi-1}}{\Delta x}\\ \frac{\partial S_w}{\partial y}&=\frac{S_{w,j+1}-S_{wj}}{\Delta y}=\frac{S_{wj}-S_{wj-1}}{\Delta y}\end{aligned} \tag{3.37}$$

Where

i	Grid Block Number in X Direction
j	Grid Block Number in Y direction

Consider equation 3.25, writing it in finite difference form we have that

$$\frac{\partial}{\partial x}(D\nabla S_w)+\frac{\partial}{\partial y}(D\nabla S_w)+\frac{\partial}{\partial t}(S_w)=0 \tag{3.38}$$

Using equation 1.31 we can write above as

$$\begin{aligned}&D_{i-\frac{1}{2}}\left[\frac{S^{n+1}{}_{wi-1}-S^{n+1}{}_{wi}}{\Delta x}\right]+D_{i+\frac{1}{2}}\left[\frac{S^{n+1}{}_{wi+1}-S^{n+1}{}_{wi}}{\Delta x}\right]+\\ &D_{j-\frac{1}{2}}\left[\frac{S^{n+1}{}_{wj-1}-S^{n+1}{}_{wj}}{\Delta y}\right]+D_{j+\frac{1}{2}}\left[\frac{S^{n+1}{}_{wj+1}-S^{n+1}{}_{wj}}{\Delta y}\right]+\frac{\partial S_w}{\partial t}=0\end{aligned} \tag{3.39}$$

Where

i-1/2, i+1/2, j-1/2, j+1/2 are the averaged values of D as explained in the next section.

Using equation 3.36, 3.39 can be transformed as

$$D_{i-\frac{1}{2}}\left[\frac{S^{n+1}{}_{wi-1}-S^{n+1}{}_{wi}}{\Delta x}\right]+D_{i+\frac{1}{2}}\left[\frac{S^{n+1}{}_{wi+1}-S^{n+1}{}_{wi}}{\Delta x}\right]+ D_{j-\frac{1}{2}}\left[\frac{S^{n+1}{}_{wj-1}-S^{n+1}{}_{wj}}{\Delta y}\right]+D_{j+\frac{1}{2}}\left[\frac{S^{n+1}{}_{wj+1}-S^{n+1}{}_{wj}}{\Delta y}\right]+\left[\frac{S_w{}^{n+1}-S_w{}^{n}}{\Delta t}\right]=0 \quad (3.40)$$

3.1.3.3 Averaging of the Diffusivity Coefficient

Consider the definition of the diffusivity coefficient.

$$D = \left(\frac{k}{\phi}\frac{\lambda_w\lambda_o}{\lambda_w+\lambda_o}\right)\frac{dP_c}{dS_w} \quad (3.41)$$

Hence averaging of the diffusivity coefficient includes averaging:

1. Absolute permeability
2. Relative permeability of both phases
3. Viscosity of both phases
4. Porosity
5. Slope of capillary pressure curve with saturation.

For example the average value $D_{i+1/2}$ can be written as

$$D_{i+1/2} = \left(\frac{k_{i+1/2}}{\phi_{i+1/2}}\frac{\lambda_{wi+1/2}\lambda_{oi+1/2}}{\lambda_{wi+1/2}+\lambda_{oi+1/2}}\right)\frac{dP_c}{dS_w}\Bigg|_{i+1/2} \quad (3.42)$$

The definition of the average diffusivity coefficients is as presented in **Table 3.1**.

Table 3.1- Averaging of the Diffusivity Coefficient.

Averaged Parameter	Parameter 1	Parameter 2
$D_{i+1/2}$	D_i	D_{i+1}
$D_{i-1/2}$	D_i	D_{i-1}
$D_{j+1/2}$	D_j	D_{j+1}
$D_{j-1/2}$	D_j	D_{j-1}

There is no unique way to choose the values of $\lambda_{i+1/2}, k_{i+1/2}$ etc. In general the values are averaged in such a way that they give the most accurate values possible for the flow rate and accumulation terms. In this case, from literature the properties are averaged as given in **Table 3.2**.

Table 3.2- Averaging of Parameters.

Averaged Parameter	Method of Averaging	Units
Absolute Permeability	Harmonic Averaging	md
Relative Permeability	Up-stream Weighting	-
Porosity	Arithmetic Averaging	-
Viscosity	Arithmetic Averaging	cp
Slope of capillary pressure curve	Arithmetic Averaging	psi

The methodology of averaging is presented in Aziz and Settari[53].

3.1.3.3.1 Harmonic Averaging

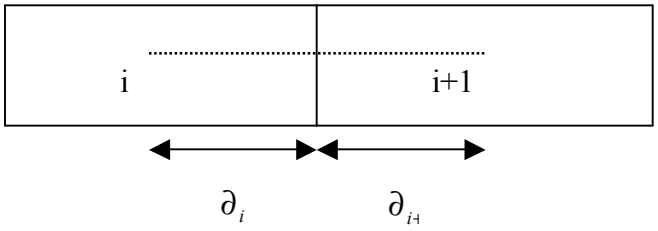

Fig. 3.3 - Averaging of permeability - harmonic averaging.

Consider a simple case of two grid blocks as shown in **Fig. 3.3**. Let us assume that the permeability is piece wise constant with interface at the block boundary. Then in case of a single fluid flow, the flow rate from grid center i to block boundary i+1/2 can be written as

$$q_{i,i+1/2} = \frac{k_i A(p_{i+1/2} - p_i)}{\mu \partial_i} \tag{3.43}$$

Similarly the flow rate from block boundary i+1/2 to block center i+1 can be written as

$$q_{i+1/2,i+1} = \frac{k_{i+1} A(p_{i+1} - p_{i+1/2})}{\mu \partial_{i+1}} \tag{3.44}$$

Since both the flow rates are equal, equating 3.43 and 3.44 and also defining an average permeability and writing the equation for flow rate from i to i+1, we have that

$$q_{i,i+1} = \frac{k_{i+1/2} A(p_{i+1} - p_i)}{\mu(\partial_i + \partial_{i+1})} = \frac{k_{i+1} A(p_{i+1} - p_{i+1/2})}{\mu \partial_{i+1}} = \frac{k_i A(p_{i+1/2} - p_i)}{\mu \partial_i} \tag{3.45}$$

Eliminating $p_{i+1/2}$ we have that

$$k_{i+1/2} = \frac{(\partial_i + \partial_{i+1})}{\frac{\partial_i}{k_i} + \frac{\partial_{i+1}}{k_{i+1}}} \tag{3.46}$$

By definition this type of averaging is called as harmonic averaging. Hence to accurately model flow, permeability needs to be harmonically averaged.

3.1.3.3.2 Arithmetic Averaging

The pressure dependent properties are assumed to be arithmetic averaged since these properties are not variable in the present case. The pressure is constant for the length of the imbibition experiment.

The capillary pressure curve slope is assumed to be arithmetic averaged[54].

3.1.3.3.3 Upstream Weighting

Upstream weighting of relative permeability and capillary pressure is a consequence of the hyperbolic nature of the problem. Raithby[55] showed that the upstream weighting leads to an accurate solution. The upstream weighting is defined as follows.

$k_{rw} = k_{rl}(S_{wi})$ if flow is from i to i+1.

and $k_{rw} = k_{rw}(S_{wi+1})$ if flow is from i+1 to i.

3.2 Derivation of Dual Porosity Flow Equations

3.2.1 Flow Equations

3.2.1.1 Fracture Flow Equations

Stating Darcy's Law for multiphase flow in porous media, we have

$$\vec{u}_w = -\frac{k\,k_{rw}}{\mu_w}\nabla\Phi_w = -\frac{k\,k_{rw}}{\mu_w}\nabla(p_w + \rho_w g h) \tag{3.47}$$

$$\vec{u}_o = -\frac{k\,k_{ro}}{\mu_o}\nabla\Phi_o = -\frac{k\,k_{ro}}{\mu_o}\nabla(p_o + \rho_o g h) \tag{3.48}$$

Since the primary flow path in dual porosity formulation is the fracture we have the Darcy's Law as follows

$$\vec{u}_{wf} = -\frac{k_f k_{rwf}}{B_{wf}\mu_{wf}}\nabla(p_{wf} + \rho_w g h) \tag{3.49}$$

$$\vec{u}_{of} = -\frac{k_f k_{rof}}{B_{of}\mu_{of}}\nabla(p_{of} + \rho_o g h) \tag{3.50}$$

From the definition of capillary pressure, the water phase pressure can be expressed in terms of oil phase pressure as

$$P_c = p_o - p_w = P_c(S_w); \qquad p_w = p_o - P_c \tag{3.51}$$

Thus 3.47 can be re-written as

$$\vec{u}_{wf} = -\frac{k_f k_{rwf}}{B_{wf}\mu_{wf}} \nabla(p_{of} - P_{cf} + \rho_w g h) \tag{3.52}$$

Consider a control volume (Secondary Porosity) of dimensions Δx, Δy as shown in **Fig. 3.1**. For the sake of brevity the subscript f is dropped in the derivation of the conservation of mass.

From conservation of mass principle, we have that

[Rate of change of mass in Control Volume = Rate of Net Influx]

Consider the control volume in figure 3.1, for the phase water we have

- Rate of change of mass of water in X direction

$$\rho_w \vec{u}_{wx} \Delta y - (\rho_w \vec{u}_{wx} + \frac{\partial}{\partial x}(\rho_w \vec{u}_{wx})\Delta x)\Delta y$$

- Similarly for the Y direction

$$\rho_w \vec{u}_{wy} \Delta x - (\rho_w \vec{u}_{wy} + \frac{\partial}{\partial x}(\rho_w \vec{u}_{wy})\Delta y)\Delta x$$

- Rate of accumulation of water

$$\frac{\partial}{\partial t}(\phi S_w \rho_w \Delta x \Delta y) + \tau$$

Where τ is the rate of flow of water from the matrix to the fracture, since the primary porosity also contributes to the accumulation of water in the fractures. Thus the conservation of mass can be written in the following form

$$\frac{\partial}{\partial t}(\phi S_w \rho_w \Delta x \Delta y) + \tau = (\rho_w \vec{u}_{wy} \Delta x - (\rho_w \vec{u}_{wy} + \frac{\partial}{\partial x}(\rho_w \vec{u}_{wy})\Delta y)\Delta x) + (\rho_w \vec{u}_{wx} \Delta y - (\rho_w \vec{u}_{wx} + \frac{\partial}{\partial x}(\rho_w \vec{u}_{wx})\Delta x)\Delta y) \tag{3.53}$$

Simplifying equation 3.53 similar to the conservation of mass as described in the earlier chapter we have,

$$\phi \frac{\partial}{\partial t}(S_w) + \tau_w = \nabla.(\vec{u}_w) \tag{3.54}$$

Similarly for oil phase we have

$$\phi \frac{\partial}{\partial t}(S_o) + \tau_o = \nabla.(\vec{u}_o) \tag{3.55}$$

Substituting equations 3.50 and 3.49 in equations 3.54 and 3.55 we have that

$$\phi \frac{\partial}{\partial t}(S_{wf}) + \tau_w = \nabla.(-\frac{k_f k_{rwf}}{B_{wf}\mu_{wf}} \nabla(p_{of} - P_{cf} + \rho_w g h)) \tag{3.56}$$

$$\phi \frac{\partial}{\partial t}(S_{of}) + \tau_o = \nabla.(-\frac{k_f k_{rof}}{B_{of}\mu_{of}} \nabla(p_{of} + \rho_o g h)) \tag{3.57}$$

We know that the sum of the saturations is unity. Hence

$$S_o + S_w = 1; S_o = 1 - S_w; \frac{\partial S_o}{\partial t} = -\frac{\partial S_w}{\partial t} \tag{3.58}$$

Simplifying equation 3.60 and 3.61 and using 3.62 in 3.61 we have that

$$-\phi \frac{\partial}{\partial t}(S_{wf}) + \tau_o = \nabla.(-\frac{k_f k_{rof}}{B_{of}\mu_{of}} \nabla(p_{of} + \rho_o g h)) \tag{3.59}$$

$$\phi \frac{\partial}{\partial t}(S_{wf}) + \tau_w = \nabla.(-\frac{k_f k_{rwf}}{B_{wf}\mu_{wf}} \nabla(p_{of} - P_{cf} + \rho_w g h)) \tag{3.60}$$

Multiplying both sides of the equation by the bulk volume we have

$$V_p \frac{\partial}{\partial t}(S_{wf}) - V_b \tau_o = \nabla.(a_o \nabla(p_{of} + \rho_o g h)) \tag{3.61}$$

$$-V_p \frac{\partial}{\partial t}(S_{wf}) - V_b \tau_w = \nabla.(a_w \nabla(p_{of} - P_{cf} + \rho_w gh)) \quad (3.62)$$

Where

a Symmetric coefficient defined as

a_w $\frac{k_f k_{rwf}}{B_{wf} \mu_{wf}} V_b$

The above equations don't consider source and sink terms like injection wells, production wells etc. To include wells into equation 3.65 and 3.66 the flow rate is added to the RHS with the convention of positive for production and negative in case of an injector. Therefore equations 3.65 and 3.66 can be rewritten as

$$V_p \frac{\partial}{\partial t}(S_{wf}) - V_b \tau_o - q_o = \nabla.(a_o \nabla(p_{of} + \rho_o gh)) \quad (3.63)$$

$$-V_p \frac{\partial}{\partial t}(S_{wf}) - V_b \tau_w - q_w = \nabla.(a_w \nabla(p_{of} - P_{cf} + \rho_w gh)) \quad (3.64)$$

3.2.1.2 Matrix Flow Equations

Consider a control volume of matrix similar to fig. 3.1. The rate of inflow into the matrix is zero as there is no flow into the matrix while the rate of outflow from the matrix into the transfer function, the conservation of mass can be written as

$$0 - \tau = \frac{\partial}{\partial t}(\phi S) \quad (3.65)$$

$$-\tau_w = \frac{\partial}{\partial t}(\phi S)_{wma} \quad (3.66)$$

$$-\tau_o = \frac{\partial}{\partial t}(\phi S)_{oma} \quad (3.67)$$

3.2.2 Empirical Transfer Function

The empirical equations are derived from the imbibition experiments that are conducted on the matrix core. To scale the time from the imbibition experiments to the field size Mattax and Kyte proposed the following transformation.

$$\left(t\frac{\sigma}{\mu_w L^2}\sqrt{\frac{k}{\phi}}\right)_{model} = \left(t\frac{\sigma}{\mu_w L^2}\sqrt{\frac{k}{\phi}}\right)_{matrixblock} \tag{3.68}$$

Therefore time can be converted to dimensionless time as

$$t_D = \left(t\frac{\sigma}{\mu_w L^2}\sqrt{\frac{k}{\phi}}\right) \tag{3.69}$$

From the imbibition data, a table of the recovery versus time is already obtained. Converting the time from the imbibition experiments to dimensionless as given by equation 3.50, and also the recovery can be converted into dimensionless form using the following equation

$$R_D = \frac{R}{V_R} \tag{3.70}$$

Therefore, from the numerical simulation of the imbibition experiment, a table of the recovery and time in dimensionless units can be obtained. Now the problem resolves in expressing the dimensional recovery in terms of the transfer function.

3.2.2.1 Expression of Transfer Function in Terms of Imbibition Recovery

DeSwaan proposed that the rate of imbibition into the fracture from the matrix could be expressed as

$$\tau = R_\alpha \lambda \int_o^t e^{-(t_D-\varepsilon)\lambda}\frac{\partial S_{wf}}{\partial \varepsilon}d\varepsilon \tag{3.71}$$

He also derived the Buckley-Leverett solution for the 1-D, 2-Phase water flooding displacement process. Considering the integral as shown above, the transfer function can be written as

$$\tau = R_\alpha \lambda \sum_{j=0}^{n}\left\{[S_{wf}(t_{j+1}) - S_{wf}(t_j)]\prod_{k=j}^{n} e^{-\lambda \Delta t_k}\right\} \tag{3.72}$$

Simplifying equation 3.76 we have

$$\tau = R_\alpha \lambda \{ Sum^{n-1} e^{-\lambda \Delta t_{Dn}} \} \tag{3.73}$$

Where

$$Sum^{n-1} = Sum^{n-2} + (S_{wf}{}^{n} - S_{wf}{}^{n-1}) e^{-\lambda \Delta t_{Dn-1}}$$

3.2.2.2 Implementation of Transfer Function in Terms of Recovery

Equation 3.65 and 3.66 combined with equation 3.77 can be written as

$$-V_p \frac{\partial}{\partial t}(S_{wf}) - \sum R_\alpha \lambda \{ Sum^{n-1} e^{-\lambda \Delta t_{Dn}} \} - q_o = \nabla.(a_o \nabla(p_{of} + \rho_o g h)) \tag{3.74}$$

$$V_p \frac{\partial}{\partial t}(S_{wf}) - \sum R_\alpha \lambda \{ Sum^{n-1} e^{-\lambda \Delta t_{Dn}} \} - q_w = \nabla.(a_w \nabla(p_{of} - P_{cf} + \rho_w g h)) \tag{3.75}$$

Therefore now the problem is reduced to a two-unknown two-equation problem.

3.2.3 Discretization of the Equations

Equation 3.67 and 3.68 can be discretized as shown in the previous chapter using the finite difference technique and the following equation can be arrived

$$\Delta a_o \Delta \Phi_o = - \frac{V_p / B_o}{\Delta t} \delta S_w + q_o + \sum R_\alpha \lambda \{ Sum^{n-1} e^{-\lambda \Delta t_{Dn}} \} \tag{3.76}$$

$$\Delta a_w \Delta \Phi_w = \frac{V_p / B_w}{\Delta t} \delta Sw + q_w + \sum R_\alpha \lambda \{ Sum^{n-1} e^{-\lambda \Delta t_{Dn}} \} \tag{3.77}$$

Where

a	Symmetric Coefficient
Φ	Potential. Defined as
$\Delta \Phi_w$	Δ(p-P_c) - $\rho_w g \Delta H$
$\Delta \Phi_o$	Δ(p) - $\rho_o g \Delta H$
Operator Δ	Defined as

$$\Delta = \frac{\partial}{\partial x} + \frac{\partial}{\partial y} \tag{3.78}$$

Writing the equations 3.81 and 3.82 after finite difference discretization, neglecting gravity we have

$$a_{ow\,i\text{-}1}^{n+1}(\Phi_{i\text{-}1}^{n+1}-\Phi_i^{n+1})+a_{oE\,i}^{n+1}(\Phi_{i+1}^{n+1}-\Phi_i^{n+1})+a_{oS\,j}^{n+1}(\Phi_{j\text{-}1}^{n+1}-\Phi_j^{n+1})+a_{oN\,j}^{n+1}(\Phi_{j+1}^{n+1}-\Phi_j^{n+1})$$
$$=-\frac{V_p/B_o}{\Delta t}(Sw^{n+1}-Sw^n)+q_o+\sum R_\alpha\lambda\{Sum^{n-1}e^{-\lambda\Delta t_{Dn}}\}$$

$$a_{ww\,i\text{-}1}^{n+1}(\Phi_{i\text{-}1}^{n+1}-\Phi_i^{n+1})+a_{wE\,i}^{n+1}(\Phi_{i+1}^{n+1}-\Phi_i^{n+1})+a_{wS\,j}^{n+1}(\Phi_{j\text{-}1}^{n+1}-\Phi_j^{n+1})+a_{wN\,j}^{n+1}(\Phi_{j+1}^{n+1}-\Phi_j^{n+1})$$
$$=\frac{V_p/B_w}{\Delta t}(Sw^{n+1}-Sw^n)+q_w+\sum R_\alpha\lambda\{Sum^{n-1}e^{-\lambda\Delta t_{Dn}}\} \qquad (3.79)$$

The equations 3.83 and 3.84 are highly non-linear. With the advent of faster computers the conventional IMPES formulation of the above equation is not necessary as the IMPES method are known for their stability problems. Hence the fully implicit option is applied. To solve the equations mentioned, Newton-Raphson's method of solution can be applied.

3.2.3.1 Newton-Raphson's Solution of Non-Linear Equations

Consider equations 3.83 and 3.84. They can be posed in the matrix form as shown below

$$\vec{A}\vec{X}=\vec{b} \qquad (3.80)$$

Where

$$\vec{X}=\begin{bmatrix}\Phi_f\\ S_{wf}\\ .\\ .\\ \Phi_f\\ S_{wf}\end{bmatrix}$$

$\vec{A}$ Coefficient Matrix

$\vec{b}$ Right Hand Side Matrix

Since both "A" and "b" matrices in 3.85 are functions of "X" matrix the system of equations is non-linear. Rewriting the equation

$$\vec{R} = \vec{A}\vec{X} - \vec{b} \tag{3.81}$$

Where R matrix is called the residual matrix. Using the Taylor's series expansion the residual matrix can be written as

$$\vec{R}^{n+1} = \vec{R}^{n} + \left(\frac{\partial \vec{R}}{\partial x}\right)^{n} (\vec{x}^{n+1} - \vec{x}^{n}) \tag{3.82}$$

Setting R^{n+1} to zero as the objective is to reduce the residual to zero, the following equation can be derived

$$\vec{R}^{k} = -\left(\frac{\partial \vec{R}}{\partial x}\right)^{k} \Delta \vec{x}^{k+1} \tag{3.83}$$

Where

Δx^{k+1} x^{k+1}-x^{k}

k Iteration counter

Equation 3.88 is similar to 3.86. Therefore the equations 3.83 and 3.84 can be posed in the form of residuals and the partial derivative in the equation 3.88 can be computed as the coefficient of the change in residual with respect to a variable and the difference matrix is to be computed.

In order to solve equation 3.88 at the beginning of every time step the value of the iteration counter is made to unity and the residuals are computed at the previous time step. Then the Jacobian matrix or the partial derivative is computed at the iteration level. The equation 3.88 is solved. With the new difference matrix, the variables is updated and checked for convergence. If not converged, the iteration counter is incremented and the process is repeated till convergence. A flow diagram is presented in **Fig. 3.4.**

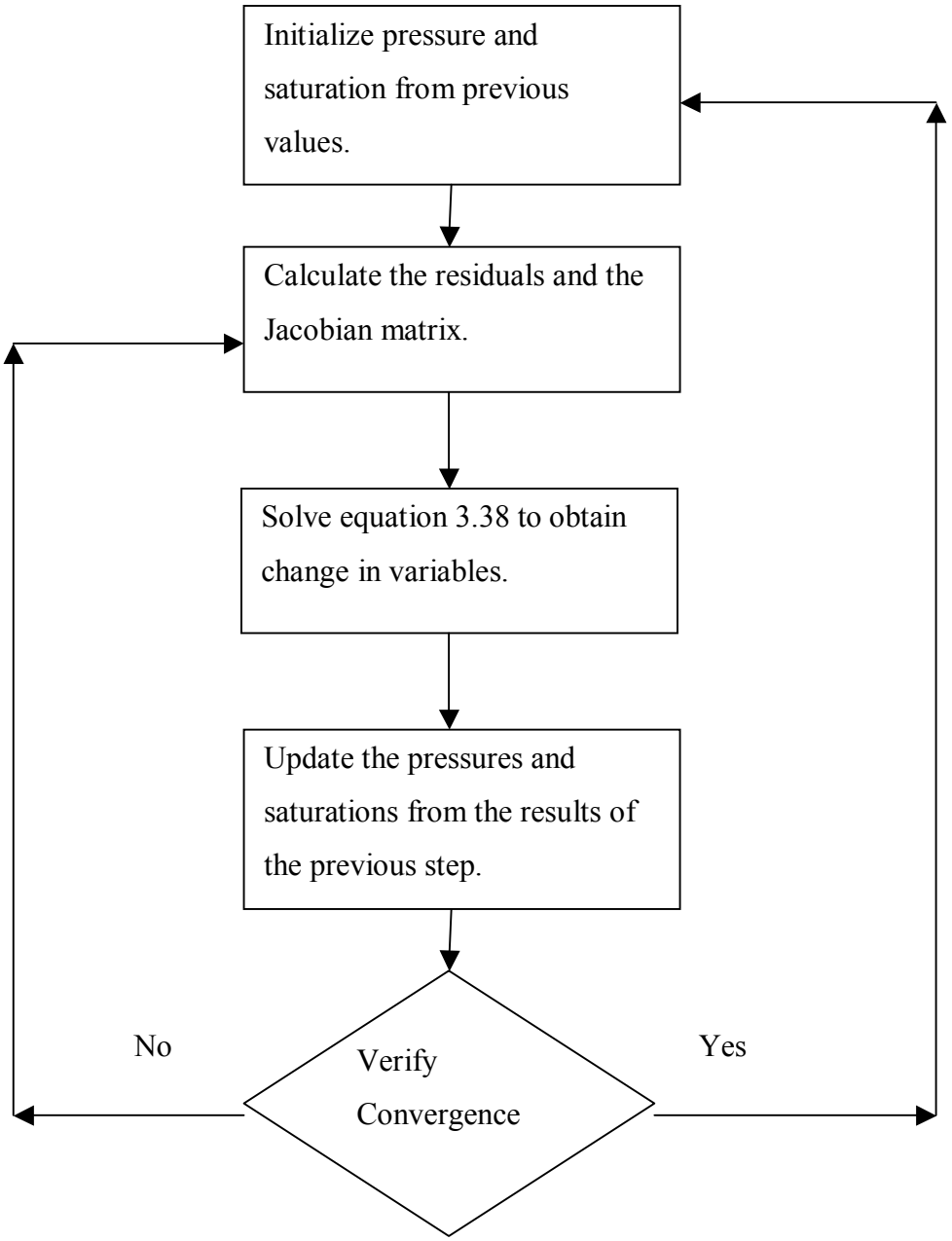

Fig. 3.4- Flow chart for Newton-Raphson's method of solution.

3.2.3.2 Posing Equations in the Residual Form

We know that both the relative permeability and capillary pressures are a function of water saturation. Therefore the coefficient "a" is not a constant but is a spatial variable of water saturation. Also using the

$$k_{ro}^{n+1} = k_{ro}^{k} + \left(\frac{k_{ro}^{n+1} - k_{ro}^{k}}{S_w^{n+1} - S_w^{k}} \right) (S_w^{n+1} - S_w^{k}) \tag{3.84}$$

$$= k_{ro}{}^{k} + k_{ro}{}' (Sw^{n+1} - Sw^{k}) \tag{3.85}$$

Where

n	Time step counter
k	Iteration counter
`	Prime operator

Therefore the symmetric coefficient can be written as

$$a_{oE}^{n+1} = a_{oE}^{k} + a_{oE}{}' (Sw^{n+1} - Sw^{k}) \tag{3.86}$$

Similarly

$$a_{wE}^{n+1} = a_{wE}^{k} + a_{wE}{}' (Sw^{n+1} - Sw^{k}) \tag{3.87}$$

Therefore equation 3.83 can be written as (ignoring gravity)

$$\left[a_{oW\,i}^{k} + a_{oW}{}'_{i} (S_{w\,i}^{n+1} - S_{wi}^{k})\right]\left(p_{i\text{-}1}^{n+1} - p_{i}^{n+1}\right) + + \left[a_{oEi}^{k} + a_{oE}{}'_{i} (S_{w\,i}^{n+1} - S_{wi}^{k})\right]\left(p_{i+1}^{n+1} - p_{i}^{n+1}\right)$$
$$+\left[a_{oS\,j}^{k} + a_{oS}{}'_{j} (S_{w\,j}^{n+1} - S_{wi}^{k})\right]\left(p_{j\text{-}1}^{n+1} - p_{j}^{n+1}\right) + + \left[a_{oN\,j}^{k} + a_{oN}{}'_{j} (S_{w\,j}^{n+1} - S_{wj}^{k})\right]\left(p_{j+1}^{n+1} - p_{j}^{n+1}\right)$$

$$= - \frac{V_p / B_o}{\Delta t} (S_{w_i}{}^{n+1} - S_{wi}^{n}) + q_o + \sum R_\alpha \lambda \{Sum^{n-1} e^{-\lambda \Delta t_{Dn}}\} \tag{3.88}$$

Now converting the unknowns to difference terms we have

$$S_w^{n+1} = S_w^{k} + S_w^{*} \tag{3.89}$$

$$p^{n+1} = p^{k} + p^{*} \tag{3.90}$$

Rewriting equation 3.93 in terms of these unknowns we have

$$\left[a^k_{oW_i} + a_{oW}{}'_i\, S^*_{wi}\right]\left(p^k_{i\text{-}1} - p^k_i + p^*_{i\text{-}1} - p^*_i\right) + \left[a^k_{oEi} + a_{oE}{}'_i\, S^*_{wi}\right]\left(p^k_{i+1} - p^k_i + p^*_{i+1} - p^*_i\right)$$
$$+\left[a^k_{oS_j} + a_{oS}{}'_j\, S^*_{wj}\right]\left(p^k_{j\text{-}1} - p^k_j + p^*_{j+1} - p^*_j\right) + \left[a^k_{oN_j} + a_{oN}{}'_j\, S^*_{wj}\right]\left(p^k_{j+1} - p^k_j + p^*_{j+1} - p^*_j\right)$$
$$= -\frac{V_p / B_o}{\Delta t}\left(S_{w_i}{}^k + S^*{}_{wi} - S^n_{wi}\right) + q_o + \sum R_\alpha \lambda \left\{Sum^{n-1} e^{-\lambda \Delta t_{Dn}}\right\} \tag{3.91}$$

Now consider the first term on the left hand side of equation 3.93

$$\left[a^k_{oW_i} + a_{oW}{}'_i\, S^*_{wi}\right]\left(p^k_{i\text{-}1} - p^k_i + p^*_{i\text{-}1} - p^*_i\right)$$
$$= a^k_{oW_i}\left(p^k_{i\text{-}1} - p^k_i\right) + a^k_{oW_i}\left(p^*_{i\text{-}1} - p^*_i\right) + a_{oW}{}'_i\, S^*_{wi}\left(p^*_{i\text{-}1} - p^*_i\right) + a_{oW}{}'_i\, S^*_{wi}\left(p^k_{i\text{-}1} - p^k_i\right)$$

The third term is a product of two differences and as the differences are small the third term can be neglected. Expanding each term in equation 3.96 and bringing the unknowns to the left hand side, the equation 3.96 can be rewritten as

$$a^k_{oW_i}\left(p^*_{i\text{-}1} - p^*_i\right) + a_{oW}{}'_i\, S^*_{wi}\left(p^k_{i\text{-}1} - p^k_i\right) + a^k_{oEi}\left(p^*_{i+1} - p^*_i\right) + a_{oE}{}'_i\, S^*_{wi}\left(p^k_{i+1} - p^k_i\right)$$
$$+ a^k_{oS_j}\left(p^*_{j\text{-}1} - p^*_j\right) + a_{oS}{}'_j\, S^*_{wj}\left(p^k_{j\text{-}1} - p^k_j\right) + a^k_{oN_j}\left(p^*_{j+1} - p^*_j\right) + a_{oN}{}'_j\, S^*_{wj}\left(p^k_{j+1} - p^k_j\right) + \frac{V_p / B_o}{\Delta t}\left(S^*{}_w\right)$$
$$= \begin{aligned} &a^k_{oW_i}\left(p^k_{i\text{-}1} - p^k_i\right) + a^k_{oEi}\left(p^k_{i+1} - p^k_i\right) + + a^k_{oS_j}\left(p^k_{j\text{-}1} - p^k_j\right) + a^k_{oN_j}\left(p^k_{j+1} - p^k_j\right) \\ &+ \frac{V_p / B_o}{\Delta t}\left(S^k{}_w - S^n{}_w\right) + q_o + \sum R_\alpha \lambda \left\{Sum^{n-1} e^{-\lambda \Delta t_{Dn}}\right\} \end{aligned} \tag{3.92}$$

The right hand side of equation 3.97, which doesn't contain any unknowns can be construed as being the residual. So the equation 3.97 can be written as

$$\vec{R}^k = -\left(\frac{\partial \vec{R}}{\partial x}\right)^k \Delta \vec{x}^{k+1} \tag{3.93}$$

Where

$$\Delta \vec{X} = \begin{bmatrix} p^* \\ S^*{}_w \\ \cdot \\ \cdot \\ p^* \\ S^*{}_w \end{bmatrix}$$

The Jacobian matrix can be computed from the coefficients of individual variables in equation 3.97. A similar equation for the water phase is

$$
\begin{aligned}
&a^k_{wW_i}(p^*_{i\text{-}1} - p^*_i) + a_{wW}{}'_i\, S^*_{wi}(p^k_{i\text{-}1} - p^k_i) + a^k_{wE_i}(p^*_{i+1} - p^*_i) + a_{wE}{}'_i\, S^*_{wi}(p^k_{i+1} - p^k_i) \\
&+ a^k_{wS_j}(p^*_{j\text{-}1} - p^*_j) + a_{wS}{}'_j\, S^*_{wj}(p^k_{j\text{-}1} - p^k_j) + a^k_{wN_j}(p^*_{j+1} - p^*_j) + a_{wN}{}'_j\, S^*_{wj}(p^k_{j+1} - p^k_j) - \frac{V_p / B_o}{\Delta t}(S^*{}_w) \\
&= \begin{aligned}[t] &a^k_{wW_i}(p^k_{i\text{-}1} - p^k_i) + a^k_{wE_i}(p^k_{i+1} - p^k_i) + + a^k_{wS_j}(p^k_{j\text{-}1} - p^k_j) + a^k_{wN_j}(p^k_{j+1} - p^k_j) \\ &- \frac{V_p / B_w}{\Delta t}(S^k{}_w - S^n{}_w) + q_w + \sum R_\alpha \lambda \{Sum^{n-1} e^{-\lambda \Delta t_{Dn}}\} \end{aligned}
\end{aligned}
\tag{3.94}
$$

3.2.3.3 Numerical Method of Estimating the Jacobian

In order to estimate the Jacobian, an alternate method can also be used. Jacobian matrix can be estimated from numerical methods as opposed to analytical methods. Consider equations 3.97 and 3.99. The Jacobian matrix for equation 3.97 (only 3.97 is considered for brevity) can be written as

$$
\vec{J} = \begin{bmatrix}
\frac{\partial R_1}{\partial p^*_1} & \frac{\partial R_1}{\partial S^*_{w1}} & \cdots & \frac{\partial R_1}{\partial p^*_n} & \frac{\partial R_1}{\partial S^*_{wn}} \\
\frac{\partial R_{1w}}{\partial p^*_1} & \frac{\partial R_{1w}}{\partial S^*_{w1}} & \cdots & \frac{\partial R_{1w}}{\partial p^*_n} & \frac{\partial R_{1w}}{\partial S^*_{wn}} \\
\cdot & \cdot & \cdots & \cdot & \cdot \\
\cdot & \cdot & \cdots & \cdot & \cdot \\
\frac{\partial R_n}{\partial p^*_1} & \frac{\partial R_n}{\partial S^*_{w1}} & \cdots & \frac{\partial R_n}{\partial p^*_n} & \frac{\partial R_n}{\partial S^*_{wn}} \\
\frac{\partial R_{nw}}{\partial p^*_1} & \frac{\partial R_{nw}}{\partial S^*_{w1}} & \cdots & \frac{\partial R_{nw}}{\partial p^*_n} & \frac{\partial R_{nw}}{\partial S^*_{wn}}
\end{bmatrix}
\tag{3.95}
$$

Consider the term in row 1 and column 1 of the Jacobian matrix, by definition, the partial differential can be written as

$$
\frac{\partial R_1}{\partial p^*{}_1} = \frac{Lt}{h \to 0}\left(\frac{R_1(p^*{}_1 + h) - R_1(p^*{}_1)}{h}\right) = \frac{Lt}{h \to 0}\left(\frac{R_1(p_1 + h) - R_1(p_1)}{h}\right)
\tag{3.96}
$$

The user can specify the value of "h" in the above equation and the limit of the ratio can be approximated as the ratio. Since the residual is continuous at zero. Therefore the partial differential can be written as

$$\frac{\partial R_1}{\partial p^*_1} = \left(\frac{R_1(p_1 + h) - R_1(p_1)}{h} \right) \tag{3.97}$$

Writing similarly for all the elements in the Jacobian matrix.

3.2.3.4 Method of Solution of the System of Equations

To solve the system of equations as posed by equation 3.98 for both the water and the oil phases, the Gaussian elimination method is proposed. Gaussian elimination is briefly described in this section.

To solve a system of equations as shown below,

$$\begin{cases} a_{11}x_1 + a_{12}x_2 + ...a_{1n}x_n = b_1 \\ a_{21}x_1 + a_{22}x_2 + ...a_{2n}x_n = b_2 \\ \qquad\qquad\qquad . \\ a_{n1}x_1 + a_{n2}x_2 + ...a_{nn}x_n = b_n \end{cases} \tag{3.98}$$

Gaussian elimination's objective is to rewrite the above equation in the following form

$$\begin{cases} \alpha_{11}x_1 + \alpha_{12}x_2 + ...\alpha_{1n}x_n = \beta_1 \\ \quad \alpha_{22}x_2 + ...\alpha_{2n}x_n = \beta_2 \\ \qquad\qquad . \\ \qquad \alpha_{nn}x_n = \beta_n \end{cases} \tag{3.99}$$

To obtain this transformation the following matrix rules are applied:

1. Interchanging of the order of the equations.
2. Multiplication of any equation by a non-zero number.
3. Addition of any equation with a multiple of any other.

After the system of equations is posed in the form indicated by 3.104, the value of x_n is first calculated using the last equation of the system, then x_{n-1} and so on till x_1 is calculated. To effect the above transformation the following method or algorithm is used:

1. Starting with the first equation, divide the equation by a_{11} to get one in the first term.
2. Subtract a_{1i} times the first equation from all the equations below the first equation to make the first term in all those equations zero.
3. Repeat the step for the second equation and so on till the last equation consists of only one term.

CHAPTER IV
DISCUSSION AND RESULTS

The objective of this chapter is to present results from the numerical models presented in the previous chapters. The results are divided into two parts:

1. The results from the imbibition experiments
2. The results from the dual porosity simulation using empirical transfer functions.

4.1 Imbibition Experiments

The formulations derived in Chapter III were used to numerically simulate the imbibition experiments of the following workers:

- Garg *et al.*[58]
- Muralidharan[59]

4.1.1 Garg Imbibition Experiment

4.1.1.1 Brief Description of Garg *et al.* Imbibition Experiment

Garg *et al.* performed a one-dimensional imbibition study on a Berea sandstone core. The properties of the core are provided in **Table 4.1**. The core was heated at 750^0 C to remove the effects of clay swelling and migration during the imbibition experiment. The core was epoxied on the sides so that imbibition occurs only from bottom to top. The fluid used was normal tap water at room temperature. The schematic of the experiment is presented in **Fig. 4.1** The Berea core was suspended from a weight balance using a steel wire into an acrylic container. The container is connected to a water tank through a rubber tube. The weight balance is connected to a data acquisition system that reads the weight of the core every second.

The water level in the container is always maintained at the bottom of the core. The weight data was acquired for 120 minutes.

4.1.1.1.1 Flow Visualization Using CT Methodology

X-ray CT was employed to map the fluid distribution in a longitudinal section of the core every 40 seconds. The core was scanned at an energy level of 140 keV and a field size of 13 cm. Slice thickness of 3 mm and a scan angle of 398^0 was used to scan the core. Before the commencement of the experiment the core was scanned to get the dry core CT number. CT scans were done every 40 seconds to obtain the CT values for a total of 520 seconds. After fully saturated with water, a CT scan was again performed to obtain the value of the CT number of the core fully saturated with water. The following equation was used to find the water saturation at any given time

$$S_w = \frac{CT_{water} - CT_{\exp}}{CT_{water} - CT_{dry}} \tag{4.1}$$

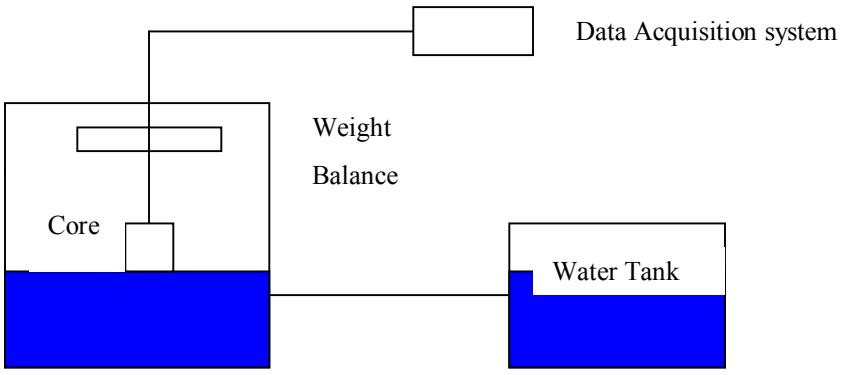

Fig. 4.1 - Experimental Setup of Garg et al. imbibition experiment.

Table 4.1- Properties of Garg's Experimental Core.

Property of the core	Value	Units
Diameter	5.46	cm
Length	6.7	cm
Porosity	0.22	-
Permeability	300	md
Initial Fluid	Air	-
Fluid Imbibed	Tap Water	-
Temperature	Room Temperature	-

4.1.1.2 Numerical Simulation of the Imbibition Experiment

In order to numerically simulate the experiment the following approximations/changes were made:

1. The core was changed from a cylindrical to cuboid shape for ease of numerical simulation.
2. The initial fluid in the core was assumed to be oil.
3. Boundary conditions were changed to reflect the one-dimensional nature of the experiment.
4. The reported imbibition was changed from weight gain to recovery of oil for matching purposes.

4.1.1.2.1 Change in Shape

The core was modified from cylindrical to cuboid for computational ease. As shown in **Fig. 4.2**, the following rules were found to be necessary and sufficient for this transformation:

1. The surface area to flow remains the same.

2. The fluids in place remain the same.

In order to keep the surface area the same, the following conversion was used.

$$\frac{\pi d^2}{4} = a^2 \tag{4.2}$$

Where

d	Diameter of the core (cm)
a	Side of the equivalent square (cm)

In order to keep the fluids in place the same the following transformation was employed.

$$\frac{\pi d^2}{4} L = a^2 h \tag{4.3}$$

Where

L	length of the cylindrical core
h	height of the equivalent cuboid.

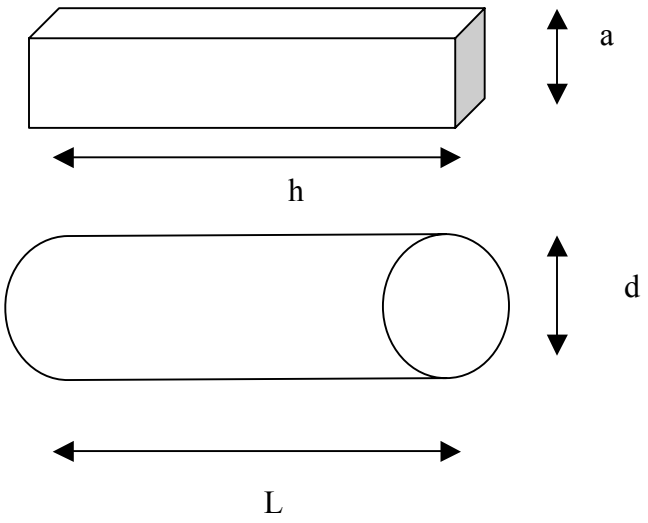

Fig. 4.2- Transformation of dimensions to accommodate change in shape.

4.1.1.2.2 Changes in the Initial Fluid Properties

Since the numerical models were developed for oil-water case, to transform it into an air-water case, the following transformations were effected:

1. Relative permeability of oil is given a value of 1 for all water saturation values.
2. Viscosity of oil is assigned a value that of air at standard conditions.
3. Density of oil is the given a value of air at standard conditions.
4. Absolute permeability was reduced to account for Klinkenberg's effect.

4.1.1.2.3 Changes in Boundary Conditions

Since Garg *et al.* performed one dimensional imbibition experiment; the boundary conditions expressed by equation 3.27 are not valid.

The core is in contact with water only at the bottom most face. Hence only the bottom most face is at constant water saturation of 1.0. All the rest of the core, prior to the experiment is at constant initial water saturation as expressed by the initial condition. Hence the boundary condition for this experiment would be

$$S_w(x, y, t) = 1, y = 0 \tag{4.4}$$

4.1.1.2.4 Changes in Reported Imbibition

The imbibition of water was reported as a function of weight gain (grams) for this experiment. Therefore, it was necessary to transform this to saturation of wetting phase. In order to obtain this transformation the following equation was used.

$$S_{wavg} = S_{wi} + \frac{62.429W}{a^2 hd} \tag{4.5}$$

Where

W	Weight gain (gms)
d	Density of water (lb/cu.ft)
a	Side of the cuboid (cm)
h	Height of the cuboid (cm)

Also the CT scanned water saturation was reported as a function of normalized height. To obtain this transformation the following was used.

$$h_{norm} = \frac{h_{actual}}{h} \tag{4.6}$$

Where

h_{norm}	Normalized height
h_{actual}	Actual Height (cm)
h	Total Height of the cuboid (cm)

4.1.1.3 Discretization of the Experiment

In order to numerically simulate the experiment, after the above transformations, the core was dicretized into a 1x1x10 grid model. An extra grid block of very small dimensions was added at the bottom to account for the boundary condition. This grid block was assigned a water saturation value of 1.0 at all times. This represents the contact of water with the core. Gravity was toggled to find the effect of gravity on the numerical simulation. The properties of the numerical case for the modeling of this experiment are as shown in **Table 4.2.**

4.1.1.4 Results from the Numerical Simulation

4.1.1.4.1 Effect of Gravity on Modeling of Imbibition Experiments

The user was given an option to include gravity in the simulation of the numerical simulation. The effect of gravity is shown in **Fig. 4.3**. For a small height of 11 cm, the effect of gravity is not prominent. The effect of gravity is not so prominent on the Garg's experiment case as the height of the core is not more than 48.3 cm. A comparison of the capillary and gravity forces is given in **Fig. 4.4.** It shows that initially the maximum capillary force is high but with time the capillary force decreases but not to an extent where it is negligible. On the other hand the maximum gravity force remains constant at 3.0E-04.

Table 4.2- Properties of the Core for Numerical Simulation.

Property	Value	Units
Number of grids blocks in X-Direction	1	-
Number of grids blocks in Y-Direction	1	-
Number of grids blocks in Z-Direction	11	-
Grid Block Dimension X-Direction	4.83	cm
Grid Block Dimension Y-Direction	4.83	cm
Grid Block Dimension Z-Direction	0.67	cm
Density of Oil	0.0006	Lb/cu.ft
Density of Water	62.4	Lb/cu.ft
Permeability X-Direction	300	md
Permeability Z-Direction	300	md
Porosity	0.22	-
Initial Water Saturation	10*0.1, 1.0	-
Boundary Condition	Bottom Most	-

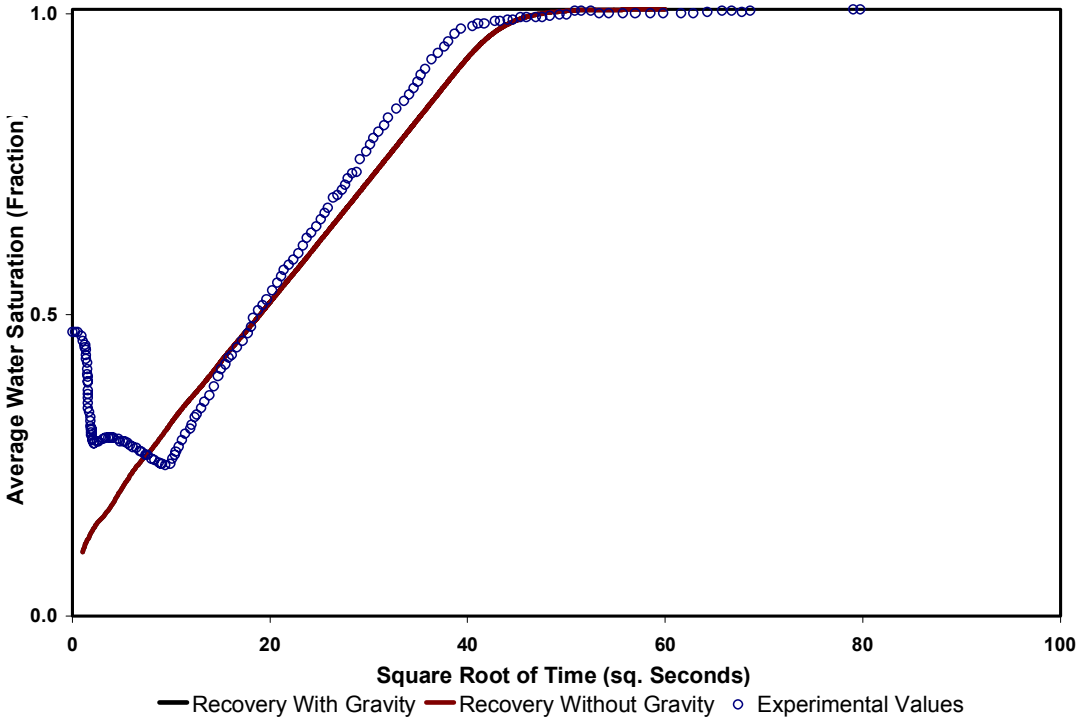

Fig. 4.3- Effect of gravity on imbibition response (Garg's imbibition experiment).

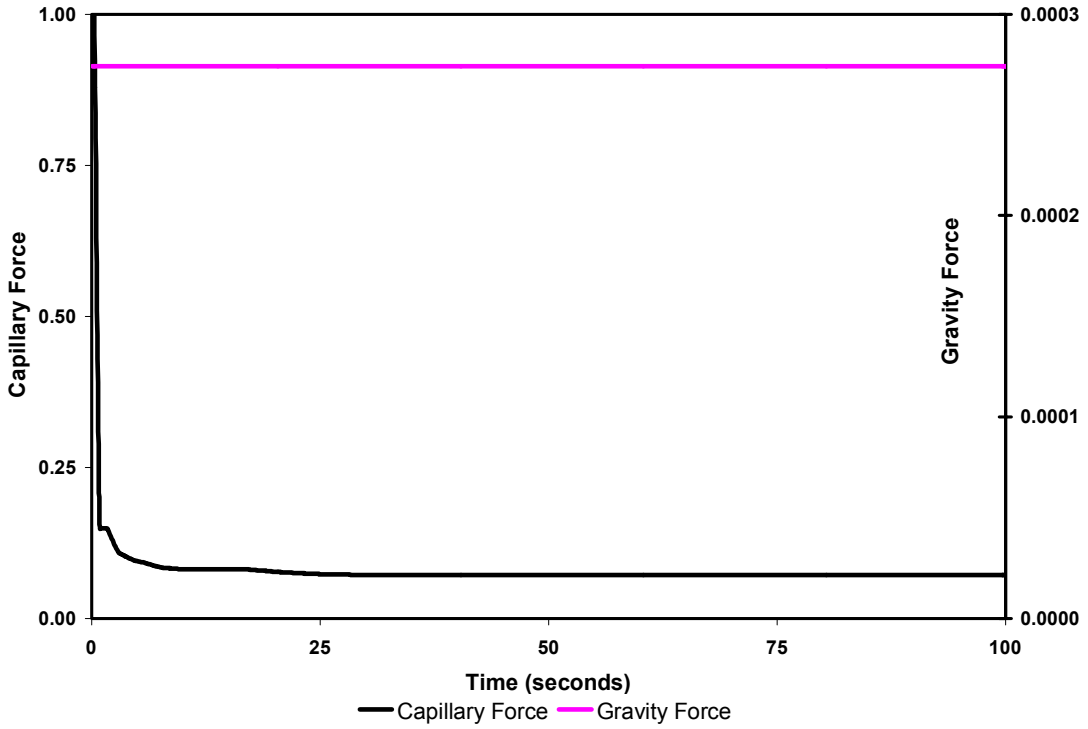

Fig. 4.4- Comparison of gravity and capillary forces.

4.1.1.4.2 Effect of Relative Permeability

Relative Permeability is modeled using a non-linear function. The function is as shown below

$$k_{rw} = k^{o}_{rw} S^{n}{}_{w} \tag{4.7}$$

The air relative permeability is assigned a value of one. Also the value of n is varied from 2 to 16 to match the recovery and also the spatial distribution of saturation. **Fig. 4.5** is a graph of the effect of relative permeability exponent "n" on the recovery. The initial portion of the experimental data, i.e from time 0 to time 100 seconds the recovery was influenced by the buoyancy forces. With sudden immersion of the core into water, the buoyancy force masked accurate values for water saturation for first 100 seconds.. From the figure, it is clear that a value of n = 8 gives the best recovery match. For all the exponents the initial portion of the recovery curve can be seen to be a straight line. Handy[57] proposed this straight-line portion. This numerical modeling proves Handy's equation. Also with increasing relative permeability exponent it can be seen that the slope

of the straight-line portion decreases. It can be seen that with change in relative permeability exponent there is no change in the final water saturation value. This final water saturation value is obtained from mass balance as 0.85, which is consistent with the reported value in the paper.

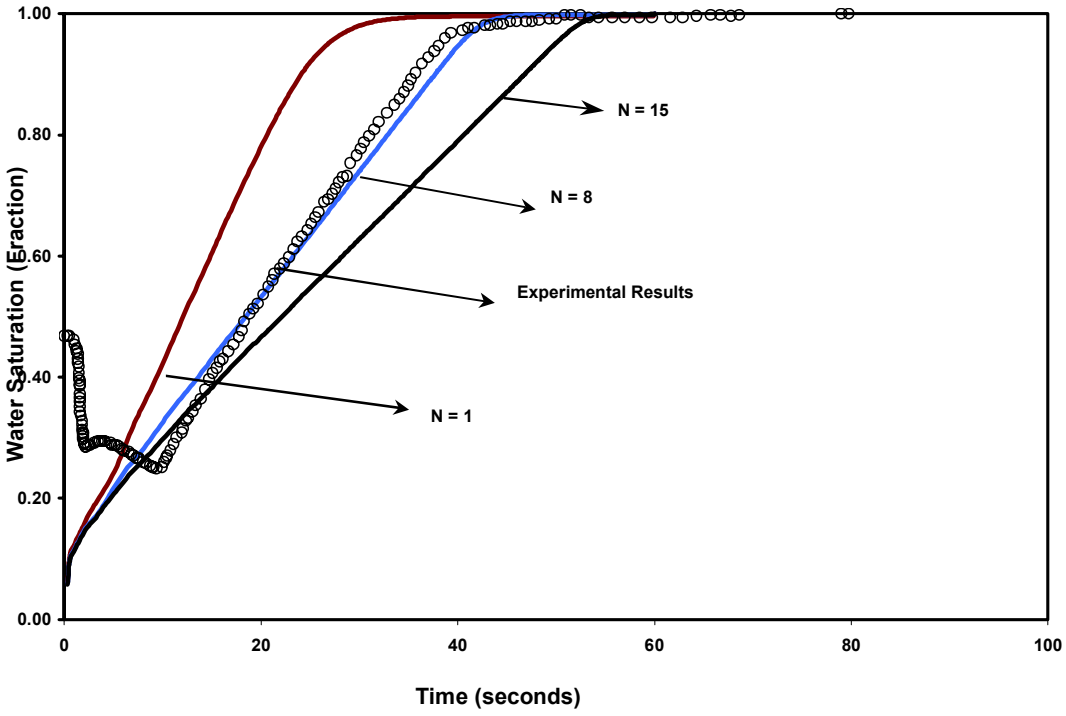

Fig. 4.5- Effect of relative permeability end point on the recovery.

4.1.1.4.3 Effect of Capillary Pressure on Imbibition

Capillary Pressure is also modeled using a non-linear function. The function is as shown below

$$P_c = P_c^0 \ln S_w \tag{4.8}$$

The capillary pressure is traditionally known to be a logarithmic function of water saturation. In this model the initial value capillary pressure or P_c^0 is varied to obtain a match of the recovery. With low capillary pressure the waterfront takes longer to reach the other end of the core. By trial and error solution the value of capillary pressure "end

point value" was found to be 40. **Fig 4.6** shows the response of imbibition experiments with change in the "end point value" of the capillary pressure.

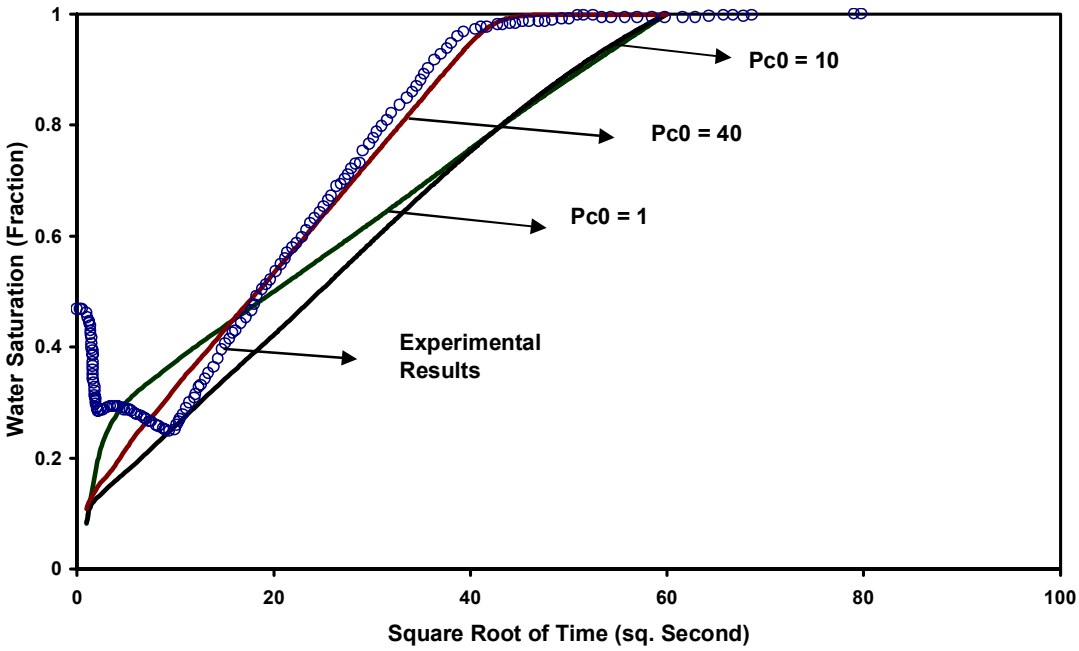

Fig. 4.6- Effect of capillary pressure on imbibition.

4.1.1.4.4 Match of the Spatial Variation of Saturation

Spatial variation of water saturation was obtained from the CT of the core during the experiment. In order to model the experiment correctly, the spatial as well as the temporal variation of the saturation should be modeled.

The spatial variation of saturation showed that there exists heterogeneity in the core at 0.3 and 0.5 times the total height. The permeability of the core was reduced to 200 md to model this heterogeneity. **Fig. 4.7** shows the match between the saturations with time as a function of normalized height as discussed in equation 4.6. The initial time steps are neglected for the match as the initial time is influenced by buoyancy as discussed in previous sections.

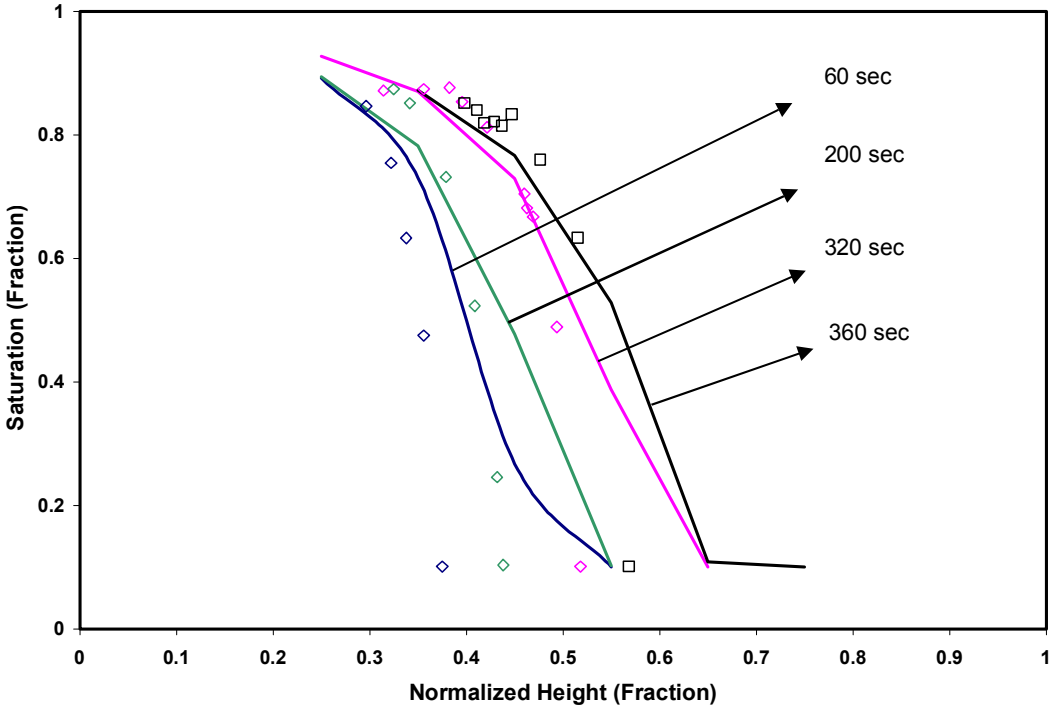

Fig. 4.7- Match between simulated and exponential variation of saturation.

4.1.2 Muralidharan Imbibition Experiment

4.1.2.1 Brief Description of Muralidharan's Experiment

Muralidharan performed a static imbibition test on Berea sandstone core **(Table 4.3)** with refined oil. His experiments dealt with overburden pressure and its effect on imbibition process. Since overburden pressure is not modeled in this study, the case for no overburden pressure is modeled using the diffusion equations generated in the previous chapter.

The air-saturated core was inserted in the "Hassler-Type" core holder. An initial overburden pressure of 500 psi was applied in the radial direction. This was followed by core flooding with the brine solution at flow rates of 5, 10, 15 and 20cc/min. The pressure drop across the core was recorded in a transducer for permeability determination. The

experiments were repeated for overburden pressures of 1000 psi and 1500 psi and the corresponding pressure drops were recorded. Subsequently, the core was flooded with oil to displace the brine. The core flooding was done till the irreducible brine saturation is achieved.

The core was then taken out of the core holder and introduced in the imbibition cell. The imbibition cell was filled with brine solution **(Table 4.4).** A simple glass container equipped with a graduated glass cap was used to gauge the imbibition experiment. The recovery of oil initially was noted every half an hour. Later the reading was taken once every 24 hours. **Fig. 4.8** shows the experiment apparatus.

Table 4.3- Physical Properties of Berea Core.

Property	**Value**	**Unit**
Diameter	3.602	Cm
Length	4.684	Cm
Area	10.190	Cm^2
Bulk Volume	47.727	Cm^3
Pore Volume	11.514	Cm^3
Porosity	24.12	Percent

Table 4.4- Brine Composition.

Salts Content	**Salt Concentration (mg/L)**
NaCl	122699
$CaCl_2.H_2O$	749
TDS	130196

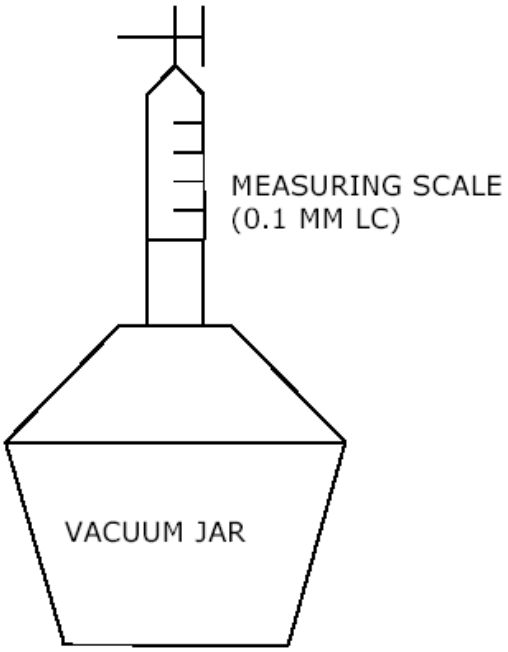

Fig. 4.8- Experimental apparatus for Muralidharan's imbibition experiment.

4.1.2.2 Numerical Simulation of Imbibition Experiment

Similar to Garg's imbibition experiment, Muralidharan's imbibition experiment was modeled using the equations derived in Chapter III. Unlike Garg's experiment, Muralidharan's experiment was not one-dimensional but three-dimensional. Hence, in order to numerically simulate the experiment the only change that was necessary was the change in shape of the core was changed from cylindrical to cuboid. The boundary conditions were the same as that stated in Chapter III.

4.1.2.2.1 Change in Shape

The core was modified from cylindrical to cuboid for computational ease. This transformation was affected using the same rules as that applied to Garg's experiment. After the transformation the numerical model for the core is as shown in **Table 4.5.**

Table 4.5- Properties of the Core for Numerical Simulation.

Property	Value	Units
Number of grids blocks in X-Direction	12	-
Number of grids blocks in Y-Direction	1	-
Number of grids blocks in Z-Direction	12	-
Grid Block Dimension X-Direction	0.3130493	cm
Grid Block Dimension Y-Direction	3.19214817	cm
Grid Block Dimension Z-Direction	0.4621	cm
Density of Oil	48.0	Lb/cu.ft
Density of Water	62.4	Lb/cu.ft
Permeability X-Direction	68	md
Permeability Z-Direction	68	md
Porosity	0. 2092	-
Initial Water Saturation	12*1,10*(1,10*0.46,1), 12*1	-
Boundary Condition	All Sides	-

4.1.2.3 Results From the Imbibition Experiment

The numerical modeling was done for the water imbibing into oil rich core case. The water is initially present in irreducible state inside the core (46%). With the start of the imbibition the oil is expelled and since there is no X-ray CT observation on this core only the recovery of oil is measured. This is matched with the experimental data by trial and error estimates of relative permeability and capillary pressures. The match of the recovery is as shown in **Fig. 4.9. Table 4.6** shows the relative permeability and capillary pressure obtained for this match.

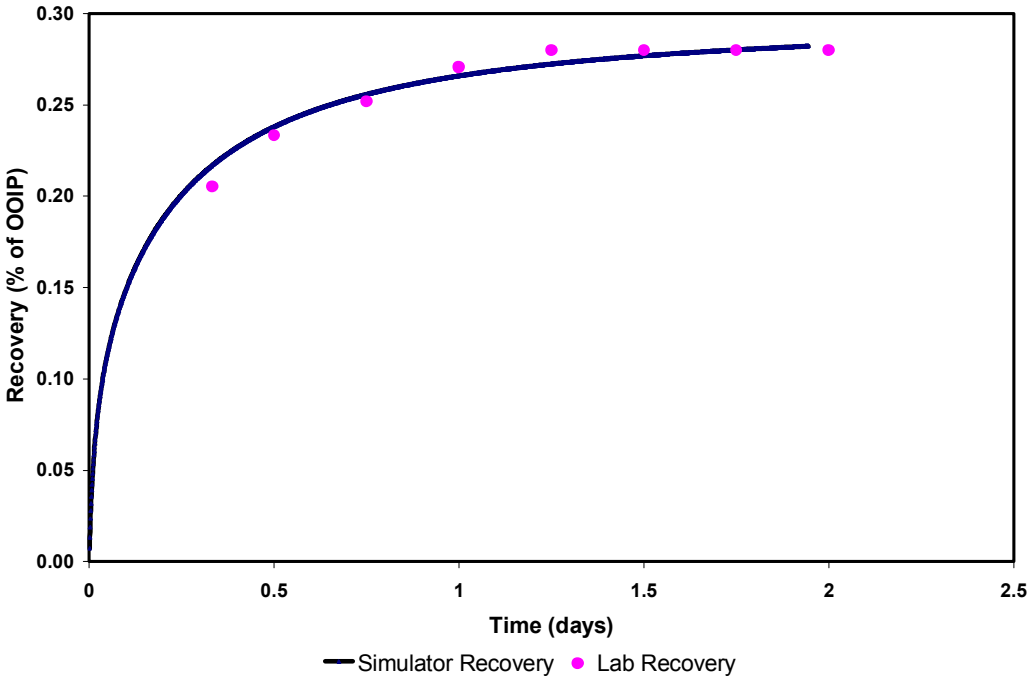

Fig. 4.9- Match of the recovery from the lab with the simulated recovery.

Table 4.6- Table of Relative Permeability.

Water Saturation (Fraction)	Water Relative Permeability	Oil Relative Permeability
0.0	0.33	0.
0.2	0.22	0.15
0.4	0.18	0.37
0.5	0.1	0.4
0.635	0.	0.44
0.76	0.	0.44
0.8	0.	0.44

Table 4.7- Table of Capillary Pressure.

Water Saturation (Fraction)	Capillary Pressure (psi)
0.14	2.0
0.2	1.71
0.4	0.91
0.5	0.653
0.6	0.518
0.635	0.46
0.76	0.11
0.8	0.1

4.2 Simulation Using Empirical Transfer Functions

Empirical transfer functions were used to model naturally fractured reservoirs and the results so obtained were compared with ECLIPSE, a commercially available simulator, which uses shape factor and Darcy's Law to model transfer of fluids. The following test cases were run:

- A one-dimensional (1x10), one well synthetic test case with two production schemes
    - Very low production rate of 1 bbl/day.
    - High production rate of 10 bbls/day.
- The one-dimensional case was converted to a two-dimensional (10x10), one well synthetic test case with very high production scheme.

4.2.1 Estimation of Empirical Parameters

To estimate the empirical parameters, a synthetic case of matrix block surrounded by water was numerically solved using the diffusion equation. This method gave the recovery as shown in **Fig. 4.17**. This recovery was curve fitted using the arfonsky's equation as stated in the previous chapter. To statistically match the arfonsky's equation, an add-in feature of Microsoft Excel called "Solver" was used. Solver was used to minimize the sum of the square of the differences to estimate the values of the empirical parameters.

4.2.2 Comparison of Results From Eclipse

To compare the results from the empirical models with ECLIPSE, the following is assumed to be necessary and sufficient to prove a good match:

1. Comparison of "Spatial Variation" of pressure.
2. Temporal variation of production rate.
3. "Spatial Variation" of water saturation.

By producing wells under a constant rate, assumption 2 is taken care of. So it is necessary to match the pressure and saturations only.

4.2.2.1 Comparison of One Dimensional Cases

After the empirical parameters were estimated, an ECLIPSE case was prepared with the petro-physical properties of the matrix block in the previous model assigned to the matrix media. Same properties were assigned to the fracture media in both the ECLIPSE case and the empirical case. A 1x10 grid block was used with a single well located at 1x1. This well was produced with two production schemes and the results compared.

Fig. 4.11 shows the pressure profile after 75 days of production from the well at 1bbl/day. The pressure profile obtained by modeling using empirical transfer function can be verified to be of the same trend and approximately of the same value as that obtained from ECLIPSE. Fig. 4.11 also shows the comparison of the two model's water saturation at the end of 75 days. The results can be verified to be similar in trend and value.

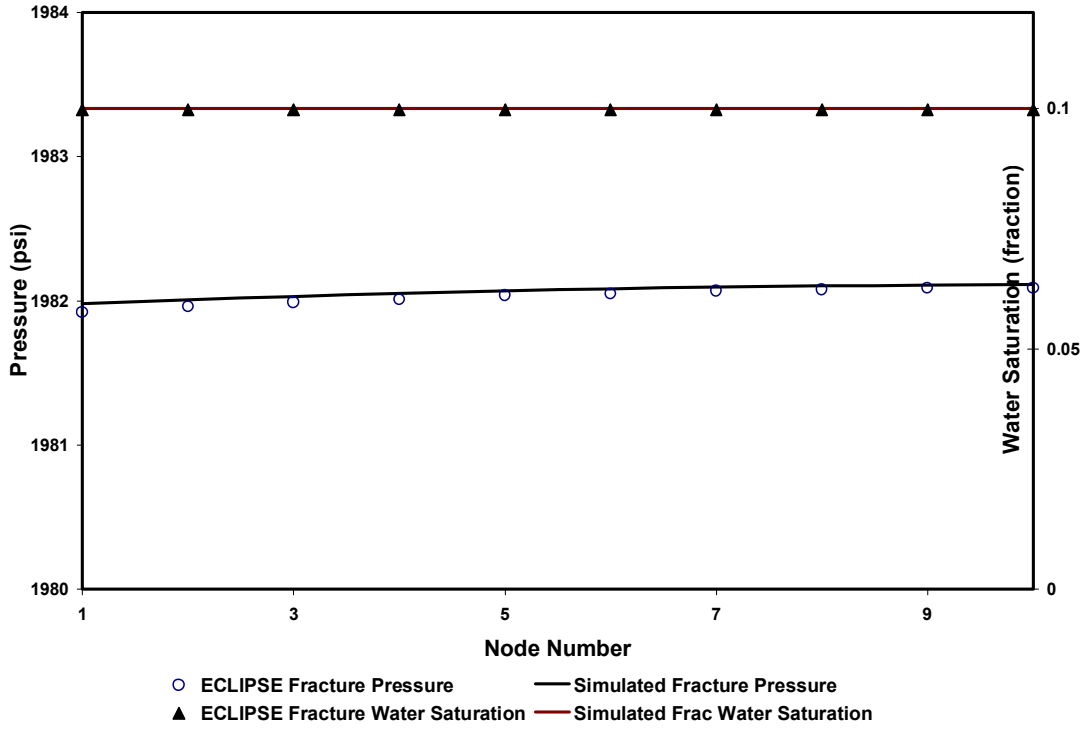

Fig. 4.11- Pressure and water saturation profiles compared with ECLIPSE.

The same reservoir model was tested for a high production rate of 10 bbls/day and the results obtained are shown in **Fig. 4.12.** The pressure of the empirical model and ECLIPSE are within error limits. Also the water saturation was found to be within the error limits for this model.

4.2.2.2 Comparison of Two-Dimensional Case

The same basic fracture system was modeled in two dimensions using a 10x10 grid. The well was placed in the center of the grid system to observe symmetry. After producing 10 bbls/day for 75 days, the results were compared with those obtained from ECLIPSE. **Fig. 4.13** shows the pressure surface of both the empirical model and ECLIPSE. It can be inferred from this figure that the pressure "effect" is greater in eclipse than from the empirical model. However the pressure profiles along a line parallel to both X and Y axes (**Fig. 4.14, Fig. 4.15**) show that the difference in pressures is within tolerable limits.

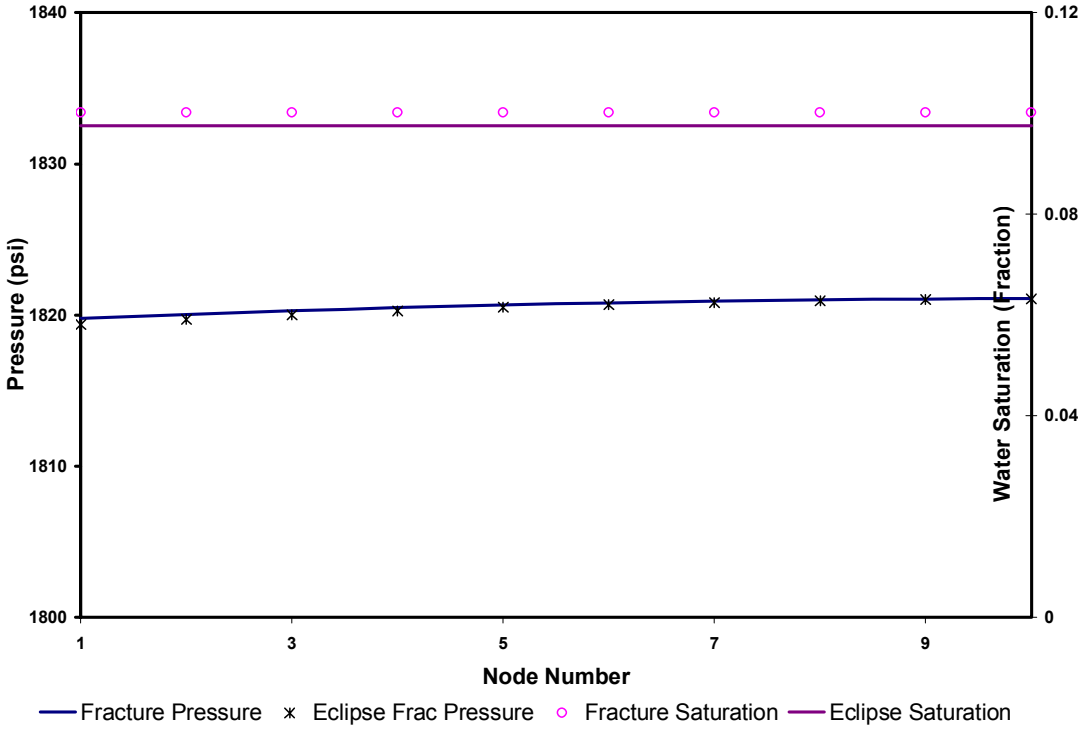

Fig. 4.12- Comparison of pressure and water saturation profiles.

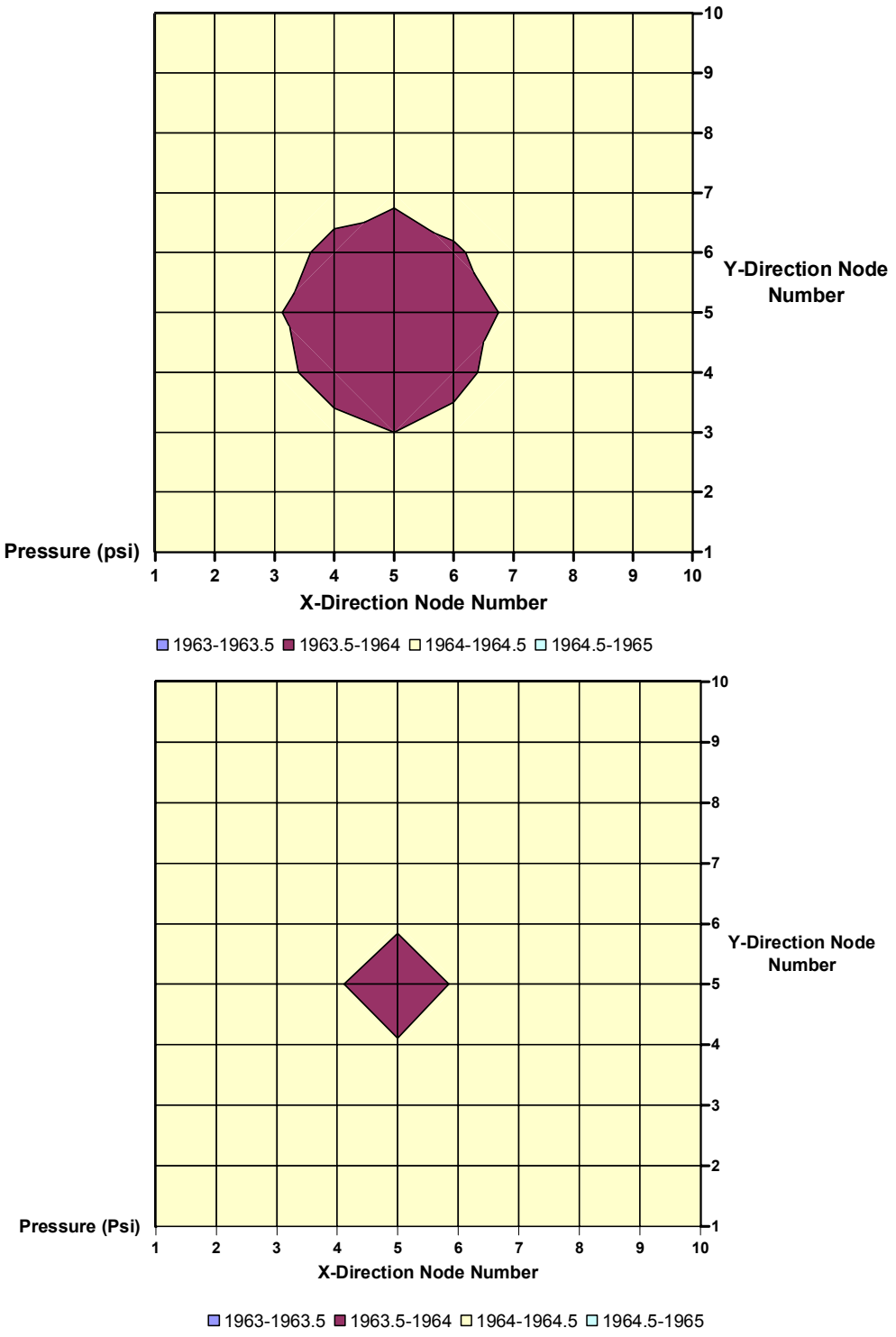

Fig. 4.13- Pressure surfaces generated by both empirical and ECLIPSE models.

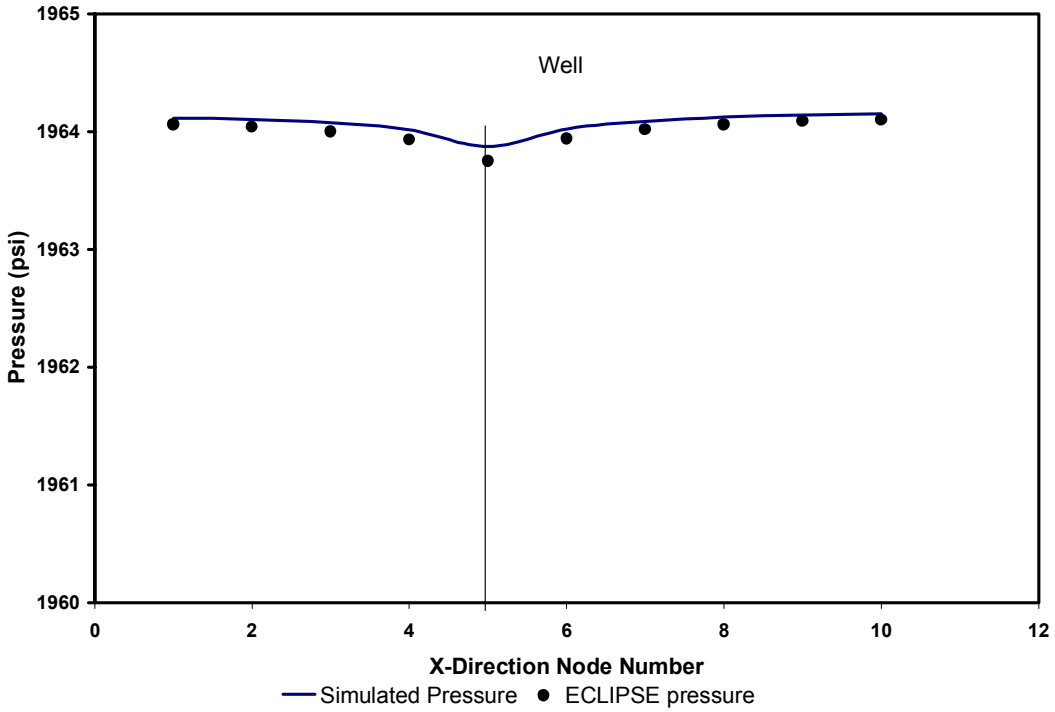

Fig. 4.14- Pressures of empirical, ECLIPSE models in a line passing parallel to X axis.

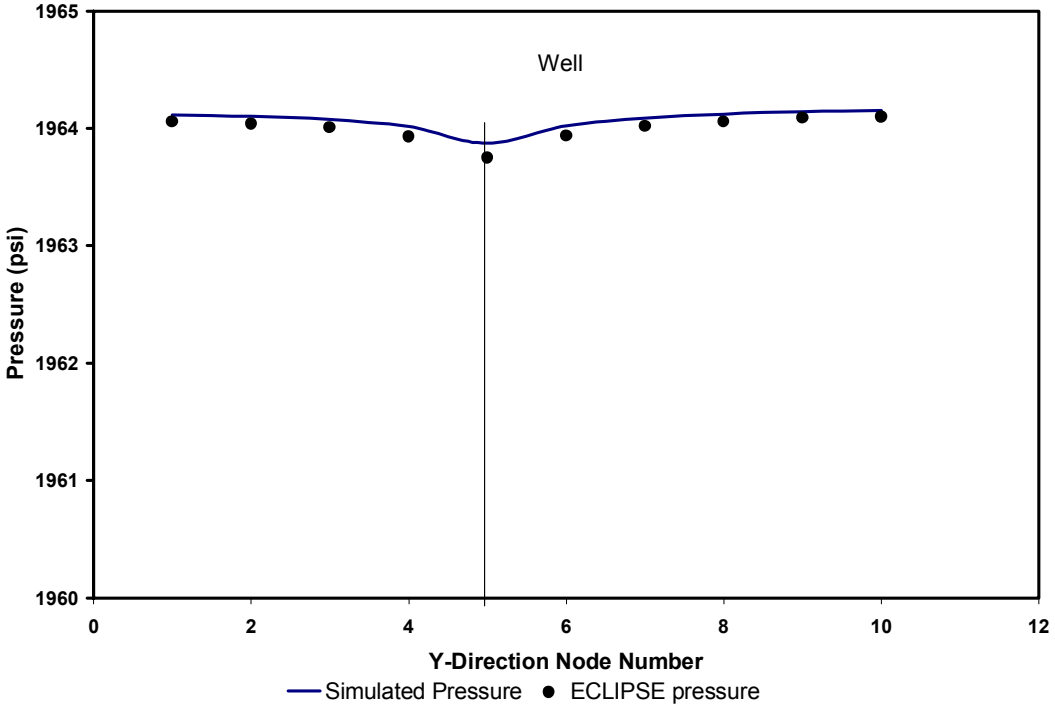

Fig. 4.15- Pressures of empirical, ECLIPSE models in a line passing parallel to Y axis.

Both **Fig. 4.14** and 4.15 are identical. This is because of the symmetry of the model. This identicalness is necessary for the formulation to be correct.

Fig. 4.17 shows the saturation surface generated by both the empirical and ECLIPSE models. It can be seen that the saturation difference is more significant than the pressure difference. This can be attributed to the difference in formulation of transfer of fluids from the matrix to the fracture.

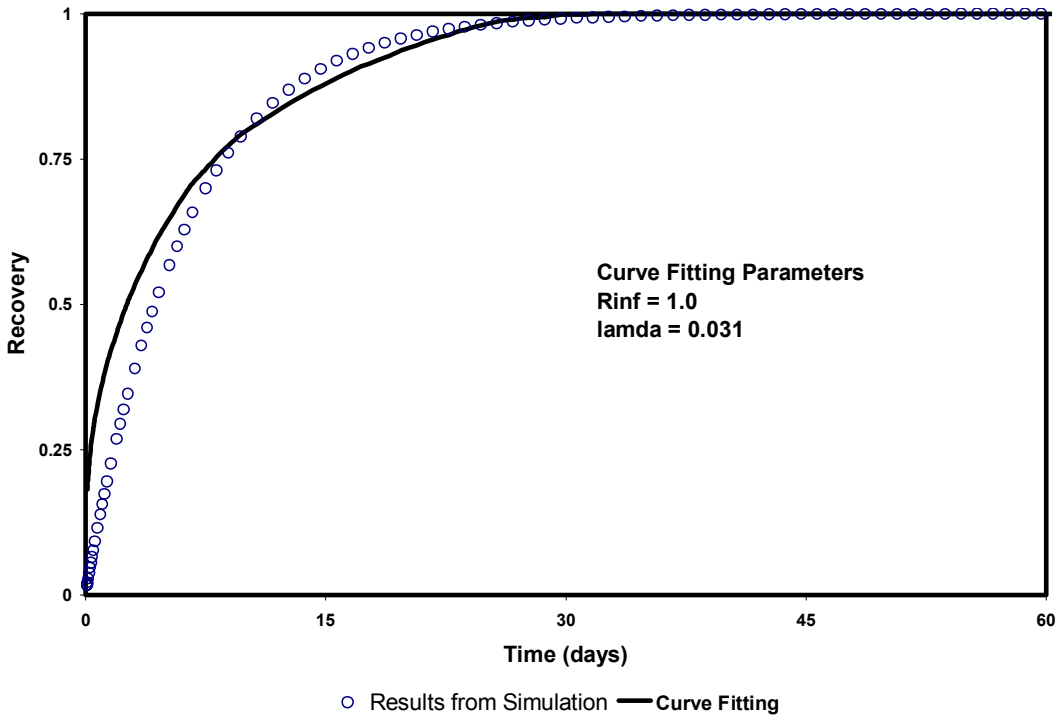

Fig. 4.16- Curve fitting recovery with exponential decline equation.

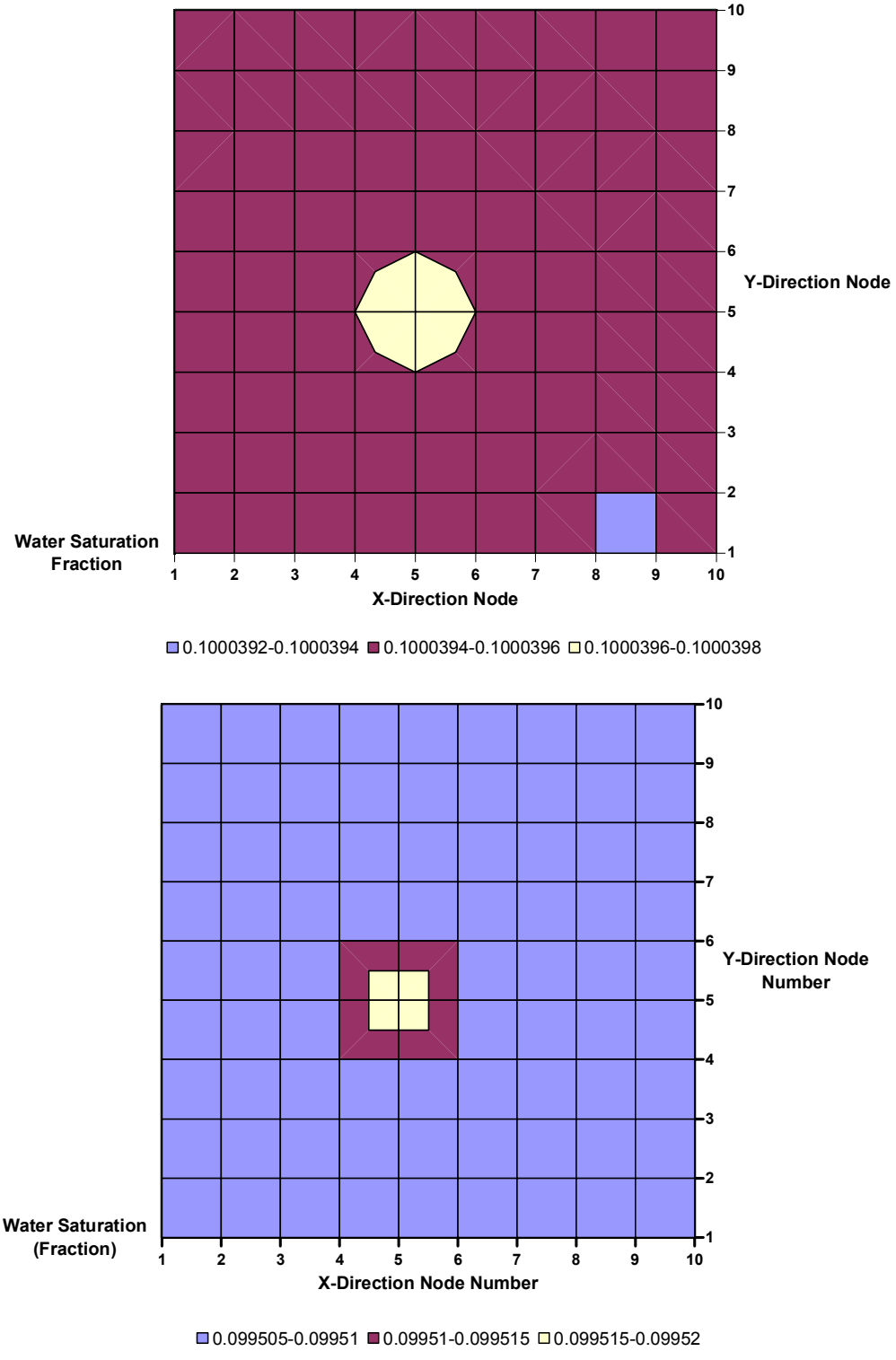

Fig. 4.17- Water saturation surfaces from both empirical and ECLIPSE models.

4.2.3 Comparison with Sub-Domain Method

Kazemi and Gilman[26] presented a 5 spot synthetic water flooding case. From this case, a grid block was selected and synthetic imbibition experiments were performed. The matrix was initially filled with recoverable oil and completely surrounded by fractures. The fracture spacing was selected in such a manner that the matrix block is of the same size as that of the grid block. Fractures that surround the matrix block were saturated with water and a field size imbibition experiment was thus created. A graphical representation of this model is shown in **Fig. 4.18.**

This model was simulated using a commercially available simulator CMG and also by the developed empirical transfer function dual porosity simulator. **Fig. 4.19** shows the matrix saturation results from the commercially available simulator and the developed simulator. "Sub-Domain" method, which is a refinement of dual porosity simulation, was also used for this test case. Sub-domain method reports the matrix saturation slightly less than that of the conventional dual porosity simulation. This is because of matrix block refinement in case of sub-domain method. In this test case, a 5 level sub-domain method was used, that is, matrix was divided into five different blocks and the average saturation of these divisions were reported as the matrix saturation.

The empirical transfer function model compares well with both these models. In the initial portion of Fig. 4.19, it can be seen that the empirical transfer function's results are within error of sub-domain method while offset from the conventional dual porosity results. This is because the conventional transfer functions formulations do not honor the initial time behavior of transfer of fluids[56]. The later time behavior of empirical transfer function model is within acceptable limits of both conventional transfer function model and sub-domain models.

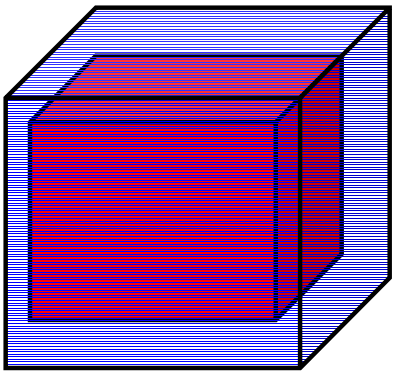

Fig. 4.18- Grid block[39] modeled using empirical and sub-domain methods.

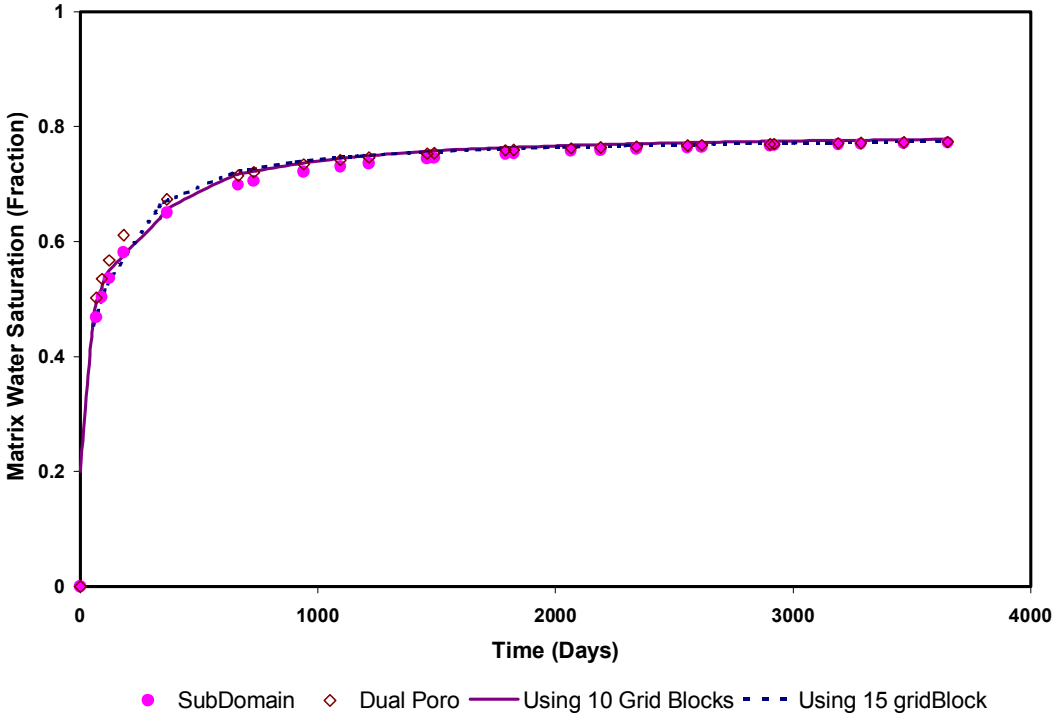

Fig. 4.19- Comparison of ETF with sub-domain method and conventional methods.

4.2.4 Limitations of Empirical Transfer Function

In its present formulation, the empirical transfer function can be used for simulation of two phase (oil-water) fluid flow. In order to extend this theory to cases where gas is also present, compressibility of gas, which is also a driving force needs to be considered. Similarly three phase flow cannot be simulated using this transfer function.

Another limitation of this theory is the limited "time step ability", that is present with this case. The integration is equation 3.71 is computed numerically using a summation term as shown in equations 3.72 and 3.73. This assumption that an integral can be accurately represented by a summation is valid only when the time steps are small. Hence very large time steps can lead to inaccurate results. A comparison of the material balance error obtained when using large steps is shown in **Fig. 4.20**. As can be seen from this graph, the oil material balance for the two dimensional case presented earlier, increases linearly with time.

Since this theory is based on Aronofsky's equation, all the assumptions inherent in Aronofsky's equation can also be extended to this theory.

4.2.5 Correlation to Well-Test Parameters

Dual porosity systems need two additional parameters for characterization than the homogeneous and isotropic reservoirs. These are called the interporosity flow coefficient and the storativity ratio usually denoted by λ and ω respectively. The storativity ratio is a measure of the fluid stored in the fracture system compared to the total fluid in the reservoir. The interporosity flow coefficient determines the inter-relation between matrix and fracture continua.

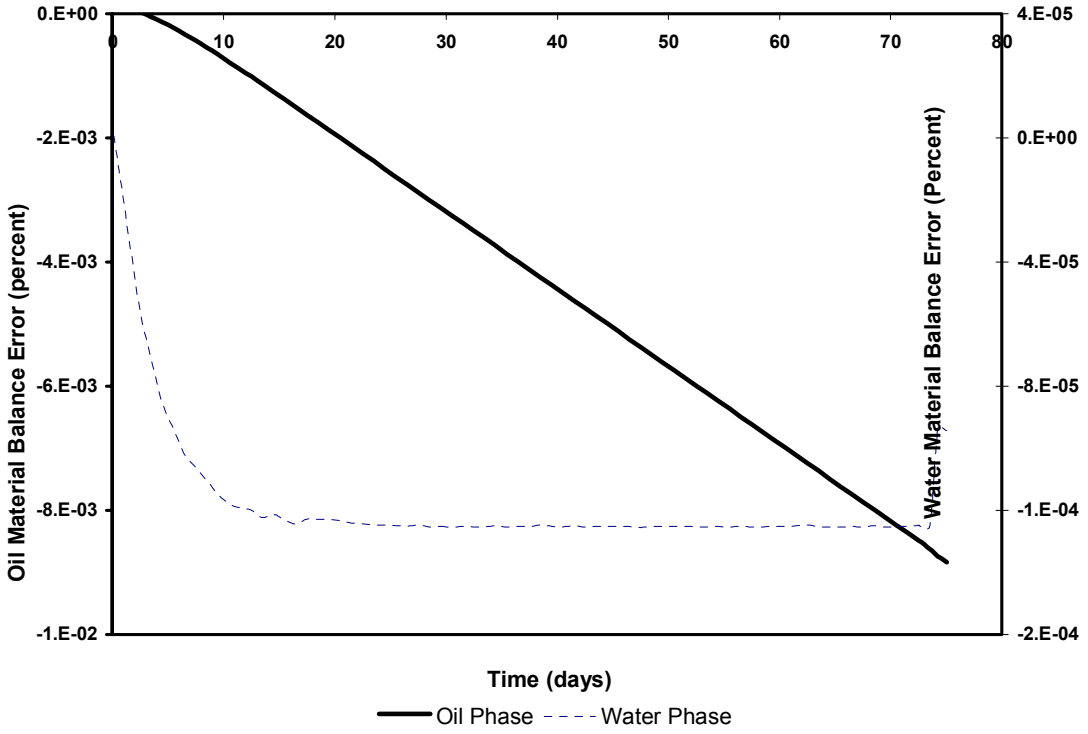

Fig. 4.20- Material balance error when using large time steps (10 days).

These two parameters, λ and ω, are usually calculated from pressure transient analysis. Their relations to the reservoir parameters are given by:

$$\lambda = \alpha \frac{k_m}{k} r_w^2 \tag{4.9}$$

$$\omega = \frac{(\phi c_t)_f}{(\phi c_t)_f + (\phi c_t)_m} \tag{4.10}$$

α is a geometric factor that depends on the shape of the matrix blocks and has dimensions of lenght^{-2}. The subscripts *m* and *f* refer to matrix and fracture systems respectively.

Higher interporosity flow coefficients indicate ease of transfer of fluids from the matrix to the fracture continua. This means that it takes lesser time for fluids to move from matrix to fracture. Recalling Aronofsky's equation, the time taken to reach the

maximum recovery value is higher in case of high exponential coefficients. (**Fig. 4.21**) Therefore proportionality can be derived between the inter-porosity flow coefficient and the exponential decay coefficient.

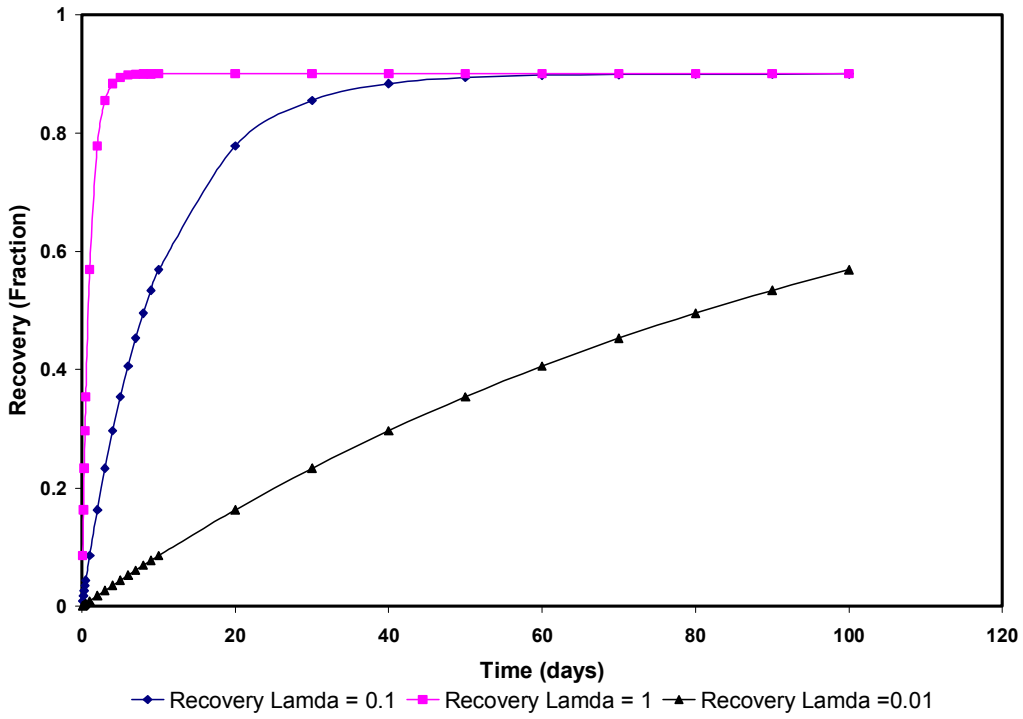

Fig. 4.21- Recovery of matrix fluid with various values of EDC.

Higher storativity ratio indicates a higher presence of fluid in fractures. For the same amount of fluid in place, an increase in storativity ratio means a reduction in the fluid in place present in the matrix blocks. But since the transfer function is expressed in terms of recovery and not actual fluid volumes, proportionality cannot be concluded between Aronofsky's parameters and storativity ratio. Further study on the relationship between these parameters is suggested as a future recommendation.

CHAPTER V

CONCLUSIONS

The following conclusions can be derived from this study:

- Diffusivity equation is sufficient to model imbibition experiments.
- Imbibition experiments provide us with empirical transfer functions that can be used to model dual porosity simulation.
- Empirical dual porosity simulation is inherently faster, since the number of unknowns per grid block is reduced to two from four.
- Empirical transfer functions model transient flow of fluids from matrix to fractures.
- Synthetic imbibition experiments can be created and modeled using diffusivity equation. Thus there is no necessity of imbibition experiments for this dual porosity formulation.
- History matching can be done by “tweaking” only one empirical transfer function parameter.

NOMENCLATURE

a = Side of a cuboid, cm

$\vec{b}$ = Right hand side matrix

ct = CT number

d = Diffusivity coefficient

e = Exponential constant, 2.7182

g = Acceleration of gravity, ft/sec^2

h = Height of core, cm

h = Formation thickness , ft

k = Absolute permeability, md

kro = Relative permeability to oil, dimensionless

krw = Relative permeability to water, dimensionless

krw^o = End-point of the relative permeability to water, dimensionless

n = Exponent of the relative permeability to water, dimensionless

N_{ma}= Number of matrix blocks

L = Fracture spacing, ft

Lf = Fracture length, ft

q = Inter-porosity flow rate, rb/day

Q = Flow rate, STB/D

p = Pressure, psia

Pc = Capillary pressure, psia

R = Recovery of oil from matrix, dimensionless

$\vec{R}$ = Residual matrix

S = Saturation of phase, fraction

t = Time, days

tD = Dimensionless time

V_R = Bulk volume, ft^3

V_P = Pore volume, ft^3

$\vec{x}$ = Matrix of unknowns in residual form

$\vec{X}$ = Matrix of unknowns in conventional form

α = Coefficients for Gaussian elimination method

β = Residuals in Gaussian elimination method.

λ_w = Mobility of water, md/cp

λ_o = Mobility of oil, md/cp

λ_T = Total Mobility, md/cp

λ = Exponential decline exponent

$\lambda_{1,2,3}$ = Civan's exponential decline constant

$\vec{u}$ = Flow rate, rb/ft^2-day

τ = Inter-porosity flow rate, ft^3/day

ϕ = Porosity, fraction

μ = Viscosity, cp

ρ = Density, lb/ft3

Φ = Flow potential, psia

σ = Shape factor, ft^{-2}

Subscripts

D = Dimensionless

f = Fracture

i = Initial value

m = Matrix

o = Oil phase

w = Water phase

x = *x*-direction

y = *y*-direction

z = *z*-direction

avg = Average

water = Value of water

dry = Value of dry sample

REFERENCES

1. Nelson R.: *Geological Analysis of Naturally Fractured Reservoirs,* second edition, Gulf Professional Publishing, St. Louis (2003).
2. Jaeger, J.S. and Cook, N.G.W.: *Fundamentals of Rock Mechanics*, third edition, Chapman and Hall Ltd., New York City (1979).
3. Aguilera, R.: *Naturally Fractured Reservoirs*, second edition, PennWell Pub. Co., Tulsa (1995).
4. Reiss, L.H.: *The Reservoir Engineering Aspects of Fractured Reservoirs*, Gulf Pub. Co., Houston (1980).
5. van Golf-Racht, T.D.: *Fundamentals of Fractured Reservoir Engineering*, Elsevier Scientific Pub. Co., Amsterdam (1982).
6. Nelson, R.A.: *Geologic Analysis of Naturally Fractured Reservoirs*, Gulf Pub. Co., Houston (1985).
7. *Rock Fractures and Fluid Flow: Contemporary Understanding and Applications*, Committee on Fracture Characterization and Fluid Flow, National Academy Press, Washington, D.C. (1996).
8. Livak, B.L.: "Simulation and Characterization of Naturally Fractured Reservoirs," paper presented at the 1985 Reservoir Characterization Technical Conference, Dallas.
9. Gilman, J.R. and Kazemi, H.: "Improved Calculations for Viscous and Gravity Displacement in Matrix Blocks in Dual-Porosity Simulators," *JPT* (January 1988) 60-70.
10. Labastie, A.: "Capillary Continuity between Blocks of a Fractured Reservoir," paper SPE 20515 presented at the 1990 SPE Annual Technical Conference and Exhibition, New Orleans, September 23-26.
11. Tan, J.C.T. and Firoozabadi, A.: "Dual-Porosity Simulation Incorporating Reinfiltration and Capillary Continuity Concepts: Part I – Single Gridcell," paper SPE 29113 presented at the 1995 SPE Reservoir Simulation Symposium, San Antonio, February 12-15.

12. Firoozabadi, A. and Ishimoto, K: "Theory of Reinfiltration in Fractured Porous Media: Part I – One-Dimensional Model," paper SPE 21796 presented at the 1991 Western Regional Meeting, Long Beach, California, March 20-22.
13. Barkve, T. and Firoozabadi, A.: "Analysis of Reinfiltration in Fractured Porous Media," paper SPE 24900 presented at the 1992 Annual Technical Conference and Exhibition, Washington, D.C., October 4-7.
14. Bourbiaux, B. and Kalaydjian, F.J.: "Experimental Study of Cocurrent and Countercurrent Flows in Natural Porous Media," *SPERE* (August 1990) 361-368.
15. Pooladi-Darvish, M. and Firoozabadi, A.: "Cocurrent and Countercurrent Imbibition in a Water-Wet Matrix Block," *SPEJ* (March 2000) 3-11.
16. McNaughton, D.A., and F.A. Garb. "Finding and Evaluating Petroleum Accumulations in Fractured Reservoir Rock." *Exploration and Economics of the Petroleum Industry*, (1975) **13**, 45-54.
17. Hohlt, R.B. "The Nature of Origin of Limestone Porosity", Colorado *School of Mines Quarterly* (1948) **4,** 5-51.
18. Lawn, B. and Wilshaw, R. "Indentation Fracture: Principles and Applications", *J. Mater. Sci.* (UK) (June 1975) **10**, 1049-81.
19. Agarwal, B., Hermansen, H., Sylte, J.E., and Thomas, L.K.: "Reservoir Characterization of Ekofisk Field: A Giant, Fractured Chalk Reservoir in the Norwegian North Sea – History Match," *SPEREE* (December 2000), 534-543.
20. Barenblatt, G.I., Zheltov, I.P., and Kochina, I.N.: "Basic Concepts in the Theory of Seepage of Homogenous Liquids in Fissured Rocks (Strata)," *J. Appl. Math. Mech.* (1960) **24**, 1286-1303.
21. Warren, J.E. and Root, P.J.: "The Behavior of Naturally Fractured Reservoirs," *SPEJ* (September 1963) 245-255.
22. Kazemi, H.: "Pressure Transient Analysis of Naturally Fractured Reservoirs with Uniform Fracture Distribution," *SPEJ* (December 1969) 451-462; *Trans*., AIME, **246**.
23. Abdassah, D. and Ershaghi, I.: "Triple-Porosity Systems for Representing Naturally Fractured Reservoirs," *SPEFE* (April 1986) 113-127.

24. Aronofsky, J.S., Masse, L., and Natanson, S.G.: "A Model for the Mechanism of Oil Recovery from the Porous Matrix Due to Water Invasion in Fractured Reservoirs," *Trans.*, AIME (1958) **213**, 17-19.
25. de Swaan, A.: "A Theory of Waterflooding in Fractured Reservoirs," *SPEJ* (April 1978) 117-122; *Trans.*, AIME, **265**.
26. Kazemi, H., Gilman, J.R., and Elsharkawy, A.M.: "Analytical and Numerical Solution of Oil Recovery From Fractured Reservoirs With Empirical Transfer Functions," *SPERE* (May 1992) 219-227.
27. Ries J. and Cil M.: "Analytical Model for Capillary Imbibition: Multidimensional Matrix Blocks," *In Situ*, (2000) **24**, No. 1, 79-106.
28. Civan, F.: "Waterflooding of Naturally Fractured Reservoirs: An Efficient Simulation Approach," paper SPE 25449 presented at the 1993 Production Operations Symposium, Oklahoma City, March 21-23.
29. Gupta, A. and Civan, F.: "An Improved Model for Laboratory Measurement of Matrix to Fracture Transfer Function Parameters in Immiscible Displacement," paper SPE 28929 presented at the 1994 SPE Annual Technical Conference and Exhibition, New Orleans, September 25-28.
30. Civan, F.: "Quadrature Solution for Waterflooding of Naturally Fractured Reservoirs," *SPEREE* (April 1998) 141-147.
31. Rapoport, L.A.: "Scaling Laws for Use in Design and Operation of Water/Oil Flow Models," *Trans*., AIME (1955) **204**, 143.
32. Mattax, C.C. and Kyte, J.R.: "Imbibition Oil Recovery from Fractured, Water-Drive Reservoirs," *SPEJ* (June 1962) 177-184.
33. Du Prey, E. L.: "Gravity and Capillary Effects on Imbibition in Porous Media" *Soc. Pet. Eng. J.* (June 1978) 195-206.
34. Ma, S., X. Zhang, and N.R. Morrow: "Influence of Fluid Viscosity on Mass, Transfer Between Rock Matrix and Fractures," paper presented at the 1995 Annual Technical Meeting of the Petroleum Society of CIM in Banff, Alberta, Canada, May 14-17.
35. Bourbiaux, B. and Kalaydjian, F.J.: "Experimental Study of Cocurrent and Countercurrent Flows in Natural Porous Media," *SPERE* (August 1990) 361-368.

36. Peñuela-Pineda, G.: "Modeling Interporosity Flow for Improved Simulation of Naturally Fractured Reservoirs," Ph.D. dissertation (2002), University of Oklahoma, Norman.
37. Thomas, L.K., Dixon, T.N., and Pierson, R.G.: "Fractured Reservoir Simulation," *SPEJ* (February 1983) 42-54.
38. Coats, K.H.: "Implicit Compositional Simulation of Single-Porosity and Dual-Porosity Reservoirs," paper SPE 18427 presented at the 1989 SPE Reservoir Simulation Symposium, Houston, February 6-8.
39. Gilman, J.R. and Kazemi, H.: "Improvements in Simulation of Naturally Fractured Reservoirs," *SPEJ* (August 1983) 695-707.
40. Lim, K.T. and Aziz, K.: "Matrix-Fracture Transfer Shape Factors for Dual-Porosity Simulators," *J. Pet. Sci. and Eng.* (1995) **13**, 169-178.
41. Quintard, M. and Whitaker, S.: "Transport in Chemically and Mechanically Heterogeneous Porous Media," *Adv. in Water Res*., (1996) **19**, No. 1, 29-60.
42. Noetinger, B. and Estebenet, T.: "Application of Random Walk Methods on Unstructured Grid to Up-Scale Fractured Reservoirs," paper presented at the 1998 European Conference on Mathematics of Oil Recovery, Peebles, Scotland, September 8-11.
43. Chen, J., M,A, Miller, and K. Sepehrnoori: "Theoretical Investigation of Countercument Imbibition in Fractured Reservoir Matrix Blocks," paper SPE 29141 presented at 1995 SPE Symposium on Reservoir Simulation, San Antonio, Texas, February 12-15.
44. Hernandez J.C. and C.P. Resales: "Imbibition as a Dispersion Process," paper SPE 23748 presented at the 1992 SPE Latin American Petroleum Engineering Conference, Caracas, Venezuela, March 8-11.
45. Hayashi, J.A. and C.P. Resales: "Visual Investigation of Imbibition Process,", paper SPE 23745 presented at the 1992 SPE Latin American Petroleum Engineering Conference, Caracas, Venezuela, March 8-11.
46. Najurieta, H.L.: "A Theory for Pressure Transient Analysis in Naturally Fractured Reservoirs," *JPT* (July 1980) 1241-1250.

47. Siddiqui, S., Hicks, P.J., Grader, A.S: "Verification of Buckley-Leverett Three Phase Theory Using Computerized Tomography", *J. Pet. Sci. and Engg.* (1996) **15**, 1-21.
48. Houndsfield, G.N: "A Method of and Apparatus for Examining a Body by Radiation Such as X- or Gamma-Radiation," Br. Patent No. 1,283,915.
49. Hunt, P.K., Engler, P. and Bajsarowicz, C.: "Computerized Tomography as a Core Analysis Tool: Applications, Instrument Evaluation and Image Improvement Techniques", *Soc. Pet. Eng. J., Formation Evaluation* (September 1988) 1203-1210.
50. Hicks, P.J., Deans, H.A., and Narayanan, K.: "Experimental Measurement of the Distribution of the Residual Oil Saturations in Heterogeneous Carbonate Cores Using X-ray Computerized Tomography,", paper CIM/SPE 9068 presented at the 1990 International Technical Meeting, Calgary, Alberta, June 10-13.
51. Peters, E.J. and Afzal, N.: "Characterization of Heterogeneities in Permeable Media with Computerized Tomography," *Soc. Pet. Eng. J.* (1990) **7**: 283-296.
52. Moss, R.M. *et al.*: "Direct Measurement of the Constituent Properties in a Dual Porosity Matrix," presented at the 1990 SCA Ann. Tech. Conf., Houston, August 2-3.
53. Aziz, K. and Settari, A.: *Petroleum Reservoir Simulation*, first edition, Applied Science Publishers, London, UK (1983).
54. Toronyi, R. M. and Forouq Ali, S. M.: " Determining Interblock Transmissibility in Reservoir Simulators," *JPT* (1979)*,* **26,** No. 1, pp. 77-78.
55. Raithby, G. D.: "A Critical Evaluation of Upstream Differencing Applied to Problems Involving Fluid Flow," *Comp. Methd. in Appl. Mech. and Engg.,* **9,** No.1, 75-103.
56. Aziz, K. and Lim, K.T.: "Matrix-Fracture Transfer Shape Factors for Dual Porosity Simualtors," *J. Pet. Sci. and Engg.* (1995) **13**, 169-178.
57. Handy, L.L.: "Determination of Effective Capillary Pressures for Porous Media from Imbibition Data," *SPEJ Petroleum Transactions*, AIME, (1960) **219**, 75-80.
58. Garg, A., Zwahlen, E. and Patzek, T.W.: "Experimental and Numerical Studies of One-Dimensional Imbibition in Berea Sandstone," paper presented at the 16th

Annual American Geophysical Union Hydrology Days, Fort Collins, Colorado, April, 15-18.

59. Muralidharan, V., Putra, E., and Schechter, D.S.: "Investigating the Changes in Matrix and Fracture Properties and Fluid Flow Under Different Stress-State Conditions," *SA Journal of Technology*, Fall 2004.

VITA

The author, Prasanna K. Tellapaneni was born in Hyderabad, India. He attended the Indian School of Mines from 1996 to 2000 and received a Bachelor of Technology in petroleum engineering in 2000. He began work toward a Master of Science in petroleum engineering at the Texas A&M University at College Station in the Fall of 2001. The address of the author is

Mr. Prasanna K. Tellapaneni,
C/O, Dr. Schechter,
3119, Texas A&M University,
College Station, TX 77840.